

What controls weathering?

Interpreting the geochemistry of Himalayan groundwaters

Giovanni Bernardi

2024-2025

Abstract

Blurb about stuff at start

Residence time calculations determined using rate constants close to equilibrium give ages of order ten years for the model which purports discharge to be the greatest control on weathering. The other model, following the null hypothesis that temperature is the greatest control on weathering, gives residence times of a similar order of magnitude but the assumption of a constant rate of reaction is likely unrealistic. Simple calculations based on yearly rainfall support the residence time obtained by both models. Estimates of free energy suggest that the weathering reactions contributing to the dissolved load in the groundwater are not close to equilibrium. As a result, it is unlikely that the fast rates of reaction used are appropriate for catchments like Melamchi. Furthermore, this suggests that the main assumption of the Maher model is not valid in this catchment. These analyses suggest that a combination of both models' is necessary to accurately model a real catchment like Melamchi.

Contents

Abstract	i
1 Introduction - Need to take out the subsection titles and shift the literature review into the introduction	1
1.1 Aims and Motivation	1
1.2 Study Dataset and Modeling	2
1.3 Weathering Fingerprints	2
2 Literature Review	4
2.1 Defining Weathering	4
2.2 Geological Controls on Weathering	5
2.3 Reaction Rates in Natural and Laboratory Settings	6
2.4 Response to Monsoonal Precipitation	6
2.5 Effects of a Changing Climate	7
3 Study Area	8
3.1 Geology and Geomorphic Setting	8
3.2 Climate	8
4 Data collection and analysis	9
4.1 Field Sampling	9
4.2 Major and Trace Element Analysis	9
4.3 Isotope Analysis	10
4.4 Estimates of Uncertainty	10
4.5 Cyclic and Hydrothermal Correction	11
5 Seasonal and Spatial Variation	13

5.1	Monsoonal Influence on Spring Chemistry	13
5.2	Spatial Concentration Changes between the Springs	15
5.3	Strontium isotopes and their Implications	17
5.4	Consistent Flow Paths Mid-Catchment	20
6	Discussion	23
6.1	Modal Decomposition Identifies Weathering Reaction	23
6.2	One-Dimensional Reactive Transport Models	25
6.2.1	Model Motivation - Do we add this into the other thing?	25
6.2.2	Fontorbe et al. (2013) - Null Hypothesis - Model	26
6.2.3	Maher Model - Correct this with respect to mike	28
6.2.4	Comparison of the Models	31
6.2.5	Constraints on Residence Time	33
6.3	Free Energy Calculations	35
6.3.1	Comparison with Residence Time	36
6.3.2	Constraints on Reaction Rate	37
References		39
7	Appendix 1: Strontium Isotopes and their Applications	47
8	Appendix 2: Derivation of reactive transport Models	48
8.1	Fontorbe et al. (2013) - Null Hypothesis - Model Derivation	48
8.2	Maher Model Derivation	50

Acknowledgements

This thesis would not have been possible without the amazing help from my supervisor, Ed Tipper. Mike Bickle and Al Knight have also been instrumental in guiding me through this Master's year. To my friends and peers, thank you for supporting me throughout. A Mamma, Papà, e la Virgi, grazie di tutto come sempre.

List of Tables

Nomenclature

Add geology eg HHCS Silicate Weathering

All the variables

1 Introduction - Need to take out the subsection titles and shift the literature review into the introduction

1.1 Aims and Motivation

Silicate weathering, whereby silicate minerals are dissolved by carbonic acid, sequesters atmospheric CO₂ over long (10⁶ year) timescales, influencing global climate regulation. The Himalayan mountain range spans more than 590,000 km², and is the source of major rivers, including the Ganges, Brahmaputra, and Indus. It is therefore a key region for understanding the global carbon cycle.

In highly erosive regions where the supply of silicate minerals far exceeds the weathering rate, silicate weathering reactions are thought to be sensitive to climate (Stallard & Edmund 1983 JGR, West et al, 2005) The dissolution kinetics of the largely silicate rocks in these catchments are thought to be sensitive to temperature and runoff because the weathering reactions have not gone to completion. Silicate weathering in the Himalayas as a result of their uplift and erosion in the Cenozoic may have contributed significantly to the global cooling over the past 40 million years (Raymo and Ruddiman, 1992; West et al, 2005, Kump et al, 2000 Ann Rev Earth Sci). Thus, it is this reported sensitivity to climate as well as their large size that makes them important to study, from both a scientific and practical perspective. However, more recent models have proposed silicate weathering is more sensitive to the hydrological cycle, than to temperature (Maher, 2011). The motivation of this project is to model these two hypotheses using groundwater samples obtained from a Himalayan catchment to determine the greatest control on weathering. This comparison will also prove useful for discussions of the nature of rates of reaction in real catchments. An added benefit will also be provided via a greater understanding of Himalayan water supplies which are essential for billions of people (Ives and Messerli, 1989).

1.2 Study Dataset and Modeling

In the present study, spring and rain samples from the Melamchi catchment are used as a case study to investigate the weathering rates in a rapidly eroding catchment. The sample dataset consists of 372 samples spanning four field campaigns over three years (2021-2024), as well as more recent year-long bi-weekly timeseries data from stream and spring samples in sites across the catchment. This dataset comprises major and trace ion concentrations, alkalinity, and radiogenic strontium isotopes from the Melamchi catchment. Spatial analysis shows that there are systematic variations in the chemical composition of the water along and away from the ridge. The possible controls on these variations, namely temperature, flow path length, lithology, dissolution rates, and evapotranspiration cannot be distinguished. As a result, the one-dimensional reactive transport models will hone in on one profile perpendicular to the ridge (Traverse 3).

Studying small catchments gives the opportunity to attribute large changes in water chemistry to seasonal climate changes like the monsoon. (Tipper et al, 2006). Two models are evaluated and pitted against each other to determine the greatest control on weathering in the Himalayas. The first model agrees with the initial 'null' hypothesis, that higher temperatures imply greater weathering intensities, and so more primary mineral dissolution (Fontorbe et al, 2013). The second model suggests that the primary control on weathering products is discharge, under the condition that fluid residence times are long enough so that fluids reach equilibrium with the solids (Maher, 2011).

1.3 Weathering Fingerprints

The weathering fingerprints of these catchments contain many unknowns, namely the residence time of the water, flow path direction and length, rate of reaction, and extent to which equilibrium is reached. Understanding residence time in particular is important because the geochemical reactions that are used to quantify weathering (and the biogeochemical ones too) are time-dependent; longer residence times promote greater solute accumulation in the water (Berner, 1978). These geochemical reactions are also controlled

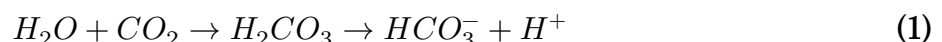
by the reaction rate which is thought to vary as equilibrium is approached (Maher, 2011). Therefore, an understanding of residence time will provide insight into the rate of reaction, and vice versa. Residence time will also reflect the variety of flow routes within a catchment, and help to constrain hydrological models.

From the model comparison will come a better understanding of fluid residence times in Himalayan catchments, for which tracer data is already commonly used to infer how long a water packet spends in the subsurface (Atwood et al, 2021). Previous studies on Melamchi have used CFC and SF₆ gases to determine a mean age on the order of ten years for groundwater at the base of the catchment ridge (Atwood et al, 2021). Using the chemical composition of the water will provide a different way of obtaining residence times, and give a benchmark for the tracer data, which is often purported to be limited in its application (McCallum et al, 2015). If the residence time of a particular water packet is long enough, it will reach chemical equilibrium, meaning the free energy of the system will be close to zero. Comparison of these residence times with estimates of free energy will provide a test on the validity of the two models and their assumptions.

2 Literature Review

2.1 Defining Weathering

As water passes through the subsurface, it interacts with rock. This causes the addition of solute species to water, and the formation of stable secondary minerals through the dissolution of primary minerals formed at different pressure and temperature. Dissolved CO₂ derived from the atmosphere present in rainfall makes it slightly acidic:



Once the rainfall enters the soil as groundwater, the acidity is further increased by the presence of decomposition of organic matter, and CO₂ production from organic activity in the soil.

The rate of weathering is dependent on the mineralogy of the rock. Different minerals weather at different rates: quartz > albite > mafic silicates > anorthite > carbonates. Therefore, the most reactive minerals will contribute disproportionately to the solute load of the water (Shand et al, 1999). In the Melamchi catchment, only the weathering of carbonic acid is considered. Sulfuric acid is also often considered a big player in weathering, but its impact is not considered in this study because the pyrite deposits required for its formation are not present in lithological studies of the Melamchi region.

Box 1: Chemical Weathering Reactions

Chemical weathering reactions are dependent on the lithology and acid content of the water. Below are the primary reactions that characterise carbonic acid weathering worldwide.

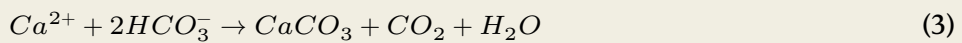
Carbonic Acid Weathering of Carbonate

This reaction has no effect on atmospheric CO₂ levels in the long term.

Short Term (10³ years):



Long Term (10⁶ years):



Carbonic Acid Weathering of Silicate

This produces net CO₂ drawdown. Reactions are written for a generic Ca-rich plagioclase mineral.

Short Term (10³ years):



Long Term (10⁷ years):



2.2 Geological Controls on Weathering

Differences in lithology are thought to affect weathering. Geological differences lead to differences in soil composition, landscape features, vegetation, and climate which in turn affect the rates of reaction. Logically, the contribution of one lithology to weathering is correlated to its spatial extent in the catchment (Stallard and Edmond, 1983). Porosities vary widely across a catchment depending on the rock type encountered (Singh et al, 1987; David et al, 1994). Porosity also increases as a rock becomes more weathered (Marques et al, 2009). Weathering regimes can be classified as either transport-limited or kinetically limited (West et al., 2005). West et al. distinguish the two regimes by the rate of erosion in the catchment. In low erosion rate settings, weathering is transport-limited due to limited

mineral supply. Weathering here is therefore proportional to the material eroded. In high erosion rate settings, weathering is kinetically limited due to an abundant mineral supply. Rapidly eroding catchments like Melamchi are therefore likely kinetically limited. Soil properties and topography are used to identify different "weathering regimes" in the subsurface (Pedrazas et al, 2021). Indeed, bedrock strength is thought to be more dependent on weathering than mineral or textural differences between the metamorphic lithologies in the Himalayas (Medwedeff et al, 2021).

2.3 Reaction Rates in Natural and Laboratory Settings

Rates of reaction during weathering comprise both dissolution and precipitation, and chemical equilibrium is defined as that state where these are balanced and equal. Rates of reaction are thought to be different depending on whether they are measured in the field or in a laboratory (Maher et al., 2009). This difference has been explained by denoting 'extrinsic' qualities that are variable in the field, such as permeability and mineral/fluid ratios (White and Brantley, 2003). The rate of reaction of a system has also been linked to the free energy of the system, with laboratory rates being calculated significantly further away from equilibrium than field rates (Kampman et al, 2009). This implies that field localities are closer to equilibrium than laboratory-derived rates might suggest.

2.4 Response to Monsoonal Precipitation

The Indian Summer Monsoon (ISM) is characterised by a strong seasonal reversal of winds, which brings heavy rainfall to the region during the summer months, and dry conditions during the winter (Bookhagen and Burbank, 2010). The monsoon brings a large amount of precipitation to the region. Oxygen isotopes suggest most of the precipitation occurs in the higher elevation parts of the catchment, and this is supported by remotely sensed rainfall estimates in the region (Acharya et al, 2020; Bookhagen and Burbank, 2010). Seasonal variation in rainfall is thought to relate to different hydrological regimes, whereby river discharge and precipitation are 'coupled' when there is a significant enough amount of water to recharge the groundwater system. (Illien et al, 2021) The seasonal variation in

precipitation therefore also translates to a variation in runoff, whereby this is twelve times stronger during the monsoon than during the dry season (Sharma, 1997).

Andermann et al. (2012) report anticlockwise hysteresis loops of precipitation against discharge (include figure?), and suggest that there is a three month lag in the response of the river to precipitation. The delay in river discharge is a topic of debate. Andermann et al. (2012) propose that at lower elevations, it is more likely due to groundwater storage of precipitation in the fractured basement. Bookhagen and Burbank (2010) suggest that the delay of precipitation and discharge may be due to the response of glaciers at higher elevations. They also suggest evapotranspiration has a low impact on the hydrological budget of the Himalayas, less than 10%. Other studies have found that catchments with little glacial input show the same delay, suggesting that the former hypothesis may be more relevant to this discussion (McGuire et al, 2005). The residence time of groundwater can hence be used to quantify this delay and nature of its origin, given that rain is the main source of recharge to the groundwater system (Illien et al, 2021).

2.5 Effects of a Changing Climate

Changes in climate contribute to changes in the monsoonal system dynamics. The start of the monsoon has not changed in Nepal, but the end has been delayed. This has led to more intense precipitation on a per day basis, which is detrimental for crops in the winter season due to lack of moisture. Intense precipitation is also considered the main climatic cause of flooding (Panthi et al, 2015; Baniya et al, 2012).

"One-off" landslide events transport as much as four times the flux of sediment deposited in the valley in a year (Chen C et al., 2023). These events are thought to be increasing in frequency over recent years as a result of climate change, increasing the erosion rate in these areas (Adhikari et al, 2023). In particular, effects of a flash flood in 2021 are still visible in the area, with damage done to several bridges and hundreds of families.

3 Study Area

The Melamchi-Indrawati catchment (85.441 - 85.601 E, 27.822 - 28.157 N) study area ranges from 790 to 5700 m a.s.l. (metres above sea level). The Melamchi River is a tributary of the larger Indrawati River and runs through the catchment draining an area of 325km².

3.1 Geology and Geomorphic Setting

The geology of Melamchi is characterised by the characteristic banded gneiss, feldspathic schist and laminated quartzite of the Higher Himalayan Crystalline Sequence (HHCS). To the south of the confluence of the Melamchi River to its parent Indrawati river lies the Main Central Thrust (MCT) which separates the HHCS from the Lower Himalayan Sequence (LHS) (Dhital et al, Graf et al). The overall geology is therefore largely comprised of silicate metamorphic rock. (map)

3.2 Climate

Annual mean temperatures in the Melamchi Khola Catchment range from 24°C at base elevation to 8°C at highest elevation sampled (3200 m a.s.l.). The area is characterised by a high erosion rate. The southern Himalayas are characterised by a large topographic gradient. This corresponds to a large temperature gradient contributing to tropical and alpine climates close to one another (Kattel et al, 2012). The westerly winds typical of this latitude are responsible for the dry season in the Himalayas (Bookhagen and Burbank, 2010). The source of precipitation during the Indian Summer Monsoon (ISM) affecting Melamchi is the Bay of Bengal, due to the strong pressure gradient that changes the westerly winds to southerly winds. This temperature gradient reverses in the winter, when the oceans are warm and the High Himalaya is cold. The Melamchi Khola catchment receives over 80% of its rainfall during the monsoon.

Catchment	Area	Mean Slope	Mean Elevation	Elevation Range	Geology	Location	Range (DD)
	(km ²)	(%)	(m)	(m)			
Melamchi Khola	325	20	2400	786–5697	HHCS	85.441–85.601 E 27.822–28.157 N	

Table 1: Catchment characteristics of the study area.

4 Data collection and analysis

4.1 Field Sampling

Both springs and rain were sampled in the field. Springs were sampled according to locations visited in past expeditions. Rain was collected in a rain gauge along several transects. Both water bodies were measured in the field for temperature, pH and TDS on a Hanna Instruments HI-991300 and EXTECH DO700. Samples were also titrated using a Hach digital titrator with 0.0625M HCl to calculate the alkalinity of the water following the Gran Method (Gran, 1952). The field measurements were done 24 hours within having been collected. Six aliquots were collected for each spring for anion, cation, titration, DIC, isotope and archive purposes respectively. Rain samples had a smaller yield and so only three aliquots were collected, for ion, isotope and archive purposes. Both water body types were filtered through a 0.2 μ m PES membrane in a filtration unit prior to bottling. Cation and archive samples were acidified with concentrated HNO₃ to give a pH of ~2, keeping the cations in solution.

4.2 Major and Trace Element Analysis

Cation concentrations were determined using a Agilent Technologies 5100 Inductively-Coupled Plasma Optical Emission Spectrometer (ICP-OES) using a calibration line made from a Nepalese spring stock solution. Anion concentrations were determined using a Dionex Ion Chromatography System (ICS) 5000 series against the Battle-02 standard calibration

line. Associated uncertainties range between 5-10% for cations and 10-15% for anions.

4.3 Isotope Analysis

Samples for radiogenic strontium analysis were dried down to provide at least 10 μg of Sr. Samples were then dissolved in aqua regia (3:1 HNO₃:HCl) to remove any additional organic matter. Once dried down again, they were added to 3 ml teflon columns with Eichrom SrSpec® resin pipetted in. Once washed three times with Milli-Q® water, the column was primed with 3M HNO₃. The sample was centrifuged then loaded onto the column avoiding any solids. The column was then washed a total of three times with 3M HNO₃ to remove other cations. Lastly, the column was eluted to a beaker with Milli-Q® water to collect the Sr. Once dried, the samples were dissolved in 3M HNO₃, centrifuged and then diluted for analysis on a Thermo Scientific Neptune Plus MC-ICP-MS. Errors on Sr isotope measurement are taken from two standard deviations of the measured values given by the MC-ICP-MS.

Samples were also analysed for stable oxygen and deuterium isotopes on a Picarro L2140-i portable analyser, using cavity ring-down spectroscopy, with an average precision of 0.05, 0.09 and 0.57 ‰ for $\delta^{17}\text{O}$, $\delta^{18}\text{O}$ and δD respectively.

4.4 Estimates of Uncertainty

Uncertainties were propagated using a Monte Carlo method. This leverages randomness to calculate uncertainties. Both observed and estimated parameters have uncertainties associated with them. Each Monte Carlo simulation randomly varies the input parameters within their estimated uncertainty ranges. Once many simulations have been run, the distribution of results reflects the possible range of values obtained for a given relationship. The uncertainty is then calculated as two standard deviations of the mean of the distribution.

4.5 Cyclic and Hydrothermal Correction

Rain input is a significant factor in the chemical composition of groundwater and rivers. Most chloride found in these water bodies is thought to be due to rainwater input (Drever, 1997). It is standard practice to correct for this cyclic input. Spring water is corrected for rain input according to the average concentration for the closest rain sample collected in this field season. To remove the contribution of the rain the following formula is used for any element X:

$$[X]_{rain-corrected} = [X]_{river} - (Cl_{river} - Cl_{river}^*) \frac{[X]_{rain}}{[Cl]_{rain}} \quad (6)$$

$$Cl_{river}^* = Cl_{river} - Cl_{rain}; \quad \text{if } Cl_{river} > Cl_{rain} \quad (7)$$

Where $[Cl]_{river}^*$ is calculated by subtracting the concentration of chloride in the rain from that in the river (Tipper et al, 2006). Cl^* is taken to be zero if the concentration of chloride in the rain is greater than concentration of river. Evapotranspiration is not considered by this model, and studies which show that it plays a minor role, accounting for less than 10% of the hydrological budget in the Himalayas (Andermann et al (2012); Bookhagen and Burbank, 2010). In those cases where Cl^* is not zero then, a primary rain correction is simply:

$$[X]_{rain-corrected} = [X]_{river} - [X]_{rain} \quad (8)$$

Once the samples have been corrected for rain input, the remaining $[Cl]^-$ is assumed to be derived from hydrothermal springs encountered in the flow path. This is likely to be the case in one of the southern traverses (Traverse 2) in Melamchi which display high chloride concentrations even after the cyclic correction. Hence, the sample with the highest $[Cl]^-$ is used to correct:

$$[X]_{hydrothermal-corrected} = [X]_{rain-corrected} - \frac{[X]}{[Cl]_{highest-Cl}} * [Cl]_{rain-corrected} \quad (9)$$

This ensures that all chloride in the corrected sample is removed. The correction uses ionic ratios from the most concentrated water source, which acts as a proxy for the sediment imparting its signature. In this way, the correction does not affect samples which do not have high Cl (and hence do not have a large hydrothermal contribution), but does decrease the concentration of ions for those that do. In the following sections, samples are plotted with the evaporite correction applied where possible. Only in those cases where no chloride was measured is the evaporite correction not applied.

5 Seasonal and Spatial Variation

5.1 Monsoonal Influence on Spring Chemistry

Concentrations of silicon in several springs in the catchment show a consistent decrease in concentration with the onset of the monsoon. Concentrations are high in April, decrease to a minimum in September, then slowly increase back to April levels through October and November. Decrease in concentration is likely a sign of dilution from increased precipitation during the monsoon. Such a trend is also present in a time series of a spring in Traverse 3. The average April-September decrease is XX% corresponding to YY mM, which is small compared to the average Si concentration of the rain, which is ZZ mM.

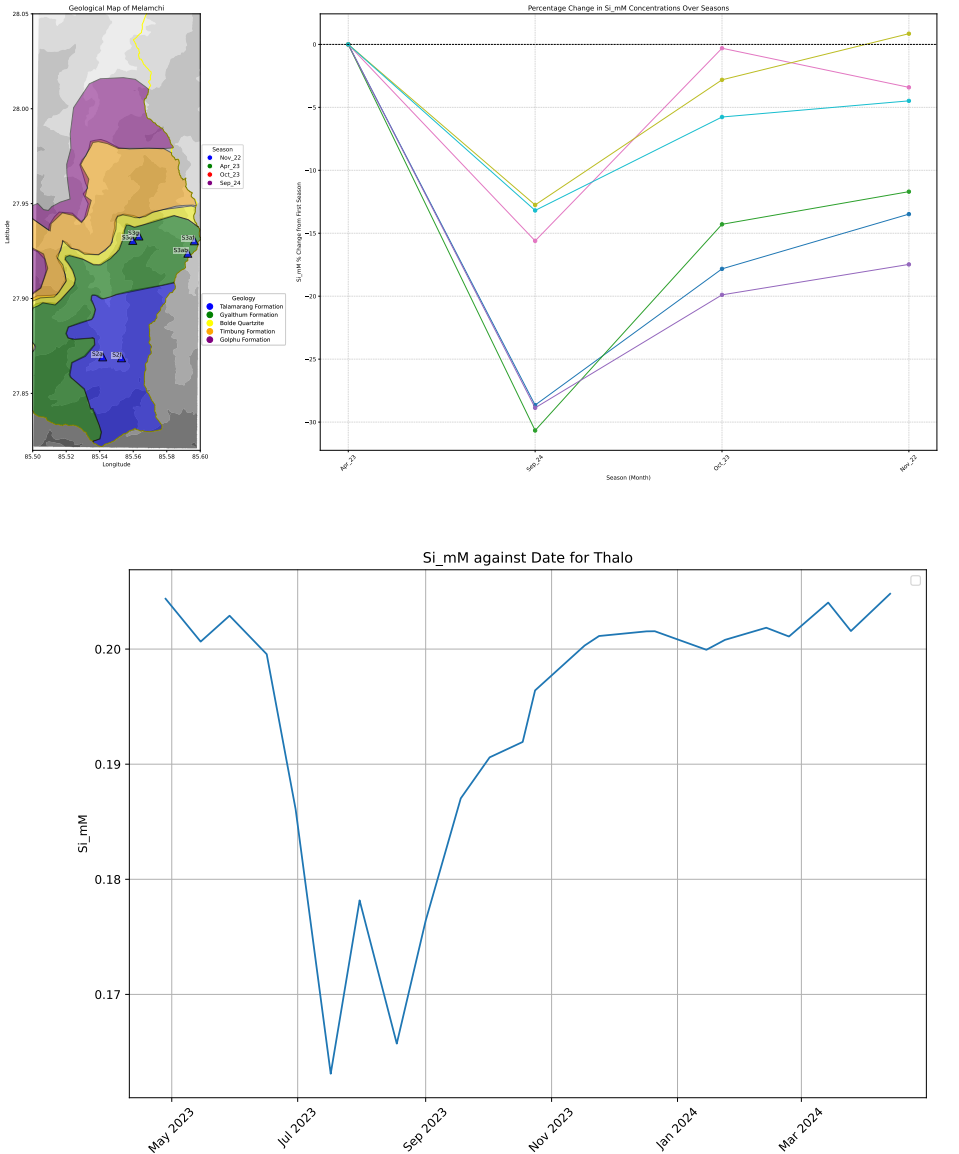


Figure 1: Seasonal changes in spring concentration indicating monsoonal precipitation influence.; Time series of spring concentration changes over time.

Recorded temperatures at the end of the spring flow paths vary with the season, being coldest in November. All seasons show a temperature decrease with increasing elevation, consistent with the free-air moist adiabatic lapse rate, which is = 6.5 °C/km (Barry and Chorley, 2009). This differs from the annual mean lapse rate in the southern Himalayas of = 5.2 °C/km (Kattel et al., 2013). This disparity could be due to the fact that temperatures may be warmer than air temperatures because of radiative heating. The difference may also be due to systematic errors in temperature measurements; between collection and sampling, warming of the water is plausible.

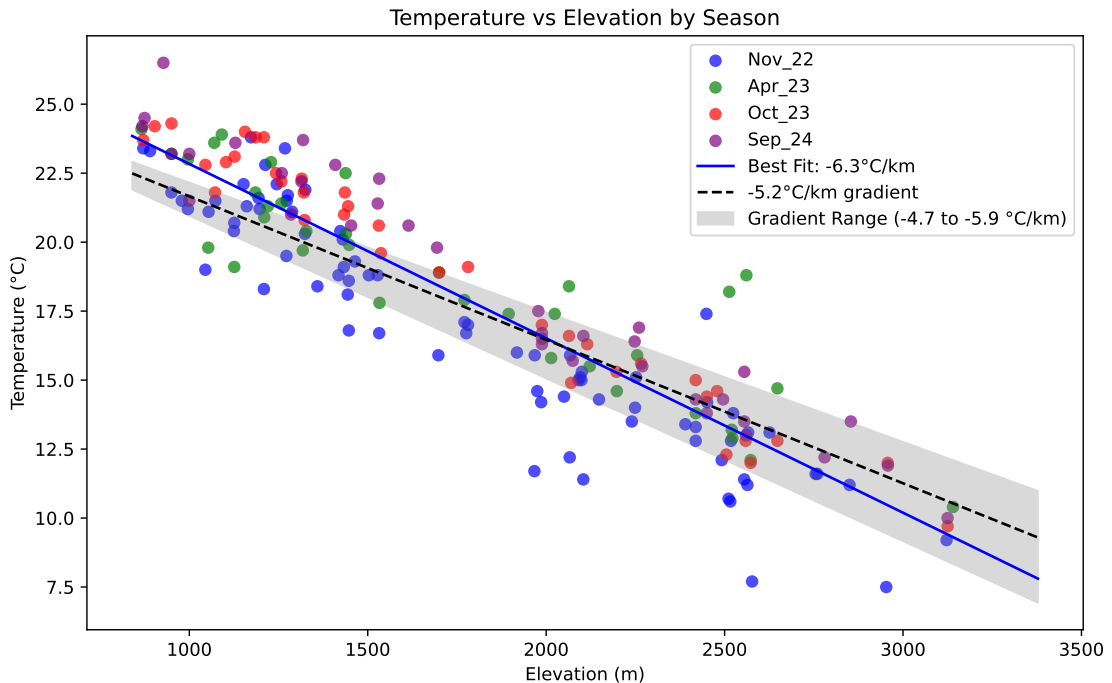


Figure 2: Temperature changes

5.2 Spatial Concentration Changes between the Springs

The northernmost three traverses display a linear trend of concentration with elevation. Alkalinity increases from the north towards the south. This suggests longer flow paths that have had more time to react and accumulate solutes. The southernmost two traverses display a distinct jump in concentration and alkalinity. Southern traverses therefore have a greater deviation from the more dilute rain signature. This could suggest that the springs sampled tap into different lithologies, but this could also be due to longer flow paths and a closer approach to equilibrium. The possible controls on these variations, namely temperature, flow path length, lithology, dissolution rates, and evapotranspiration cannot easily be distinguished.

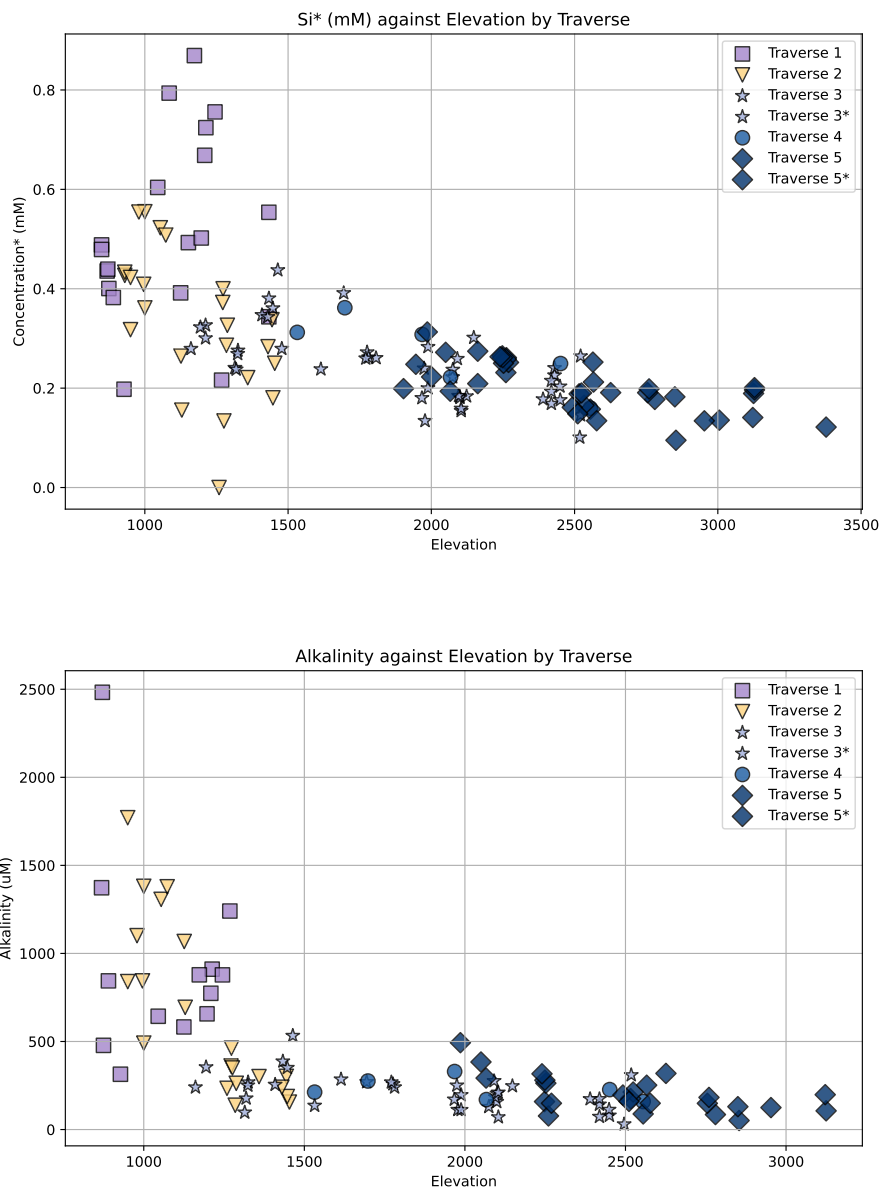


Figure 3: How Alkalinity and Si changes with elevation

5.3 Strontium isotopes and their Implications

Radiogenic strontium isotope analyses of springs also show a wide variation between different traverses. Due to the unique source-tracking nature of strontium isotopes this is potentially explained with varying lithology along the ridge. These variations are however consistent with the range of Higher Himalayan Crystalline Series (HHCS) rocks found in the region, so it is unlikely that the source of the Sr isotopes is from the Lesser Himalayan Series (LHS) rocks (Tipper et al., 2006). Indeed the Main Central Thrust (MCT) is several km south of Melamchi.

Sr isotopes measured for the collected rain samples range from 0.70904 to 0.73906. Aside from the rain sample collected in the southern Melamchi valley, the Sr isotope values are consistent with the expected values for rainwater (Galy, France-Lenord, Derry, 1999). Furthermore, the lowest Sr isotope value for rain is very close to the reported value for seawater, which is 0.70917. The lowest rain values therefore reflect seawater strontium isotope values, indicating little contamination from dust or particles. The uncontaminated samples are indeed found at the higher elevations, and they show low chloride concentrations consistent with rain.

Need to go and look at errors more accurately than this.....

Strontium isotope ratios used alongside strontium concentrations can be used to determine mixing between different endmembers (Faure, 1986; See Appendix). Plots of $\frac{^{87}Sr}{^{86}Sr}$ against $\frac{1}{Sr}$ that yield straight lines are indicative of mixing trends.

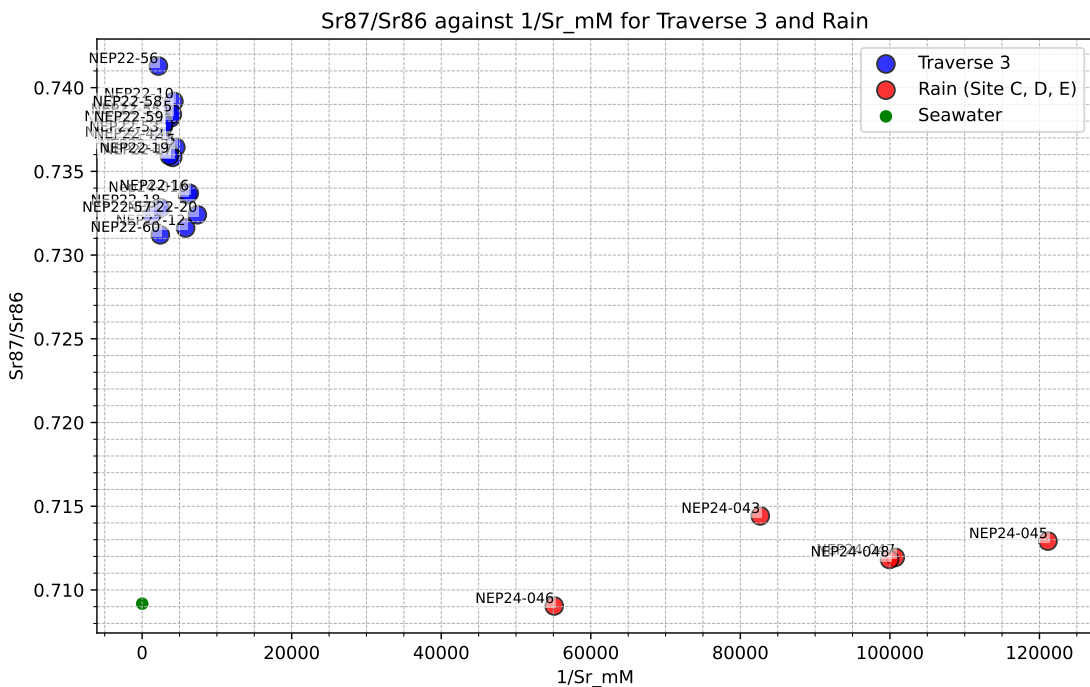
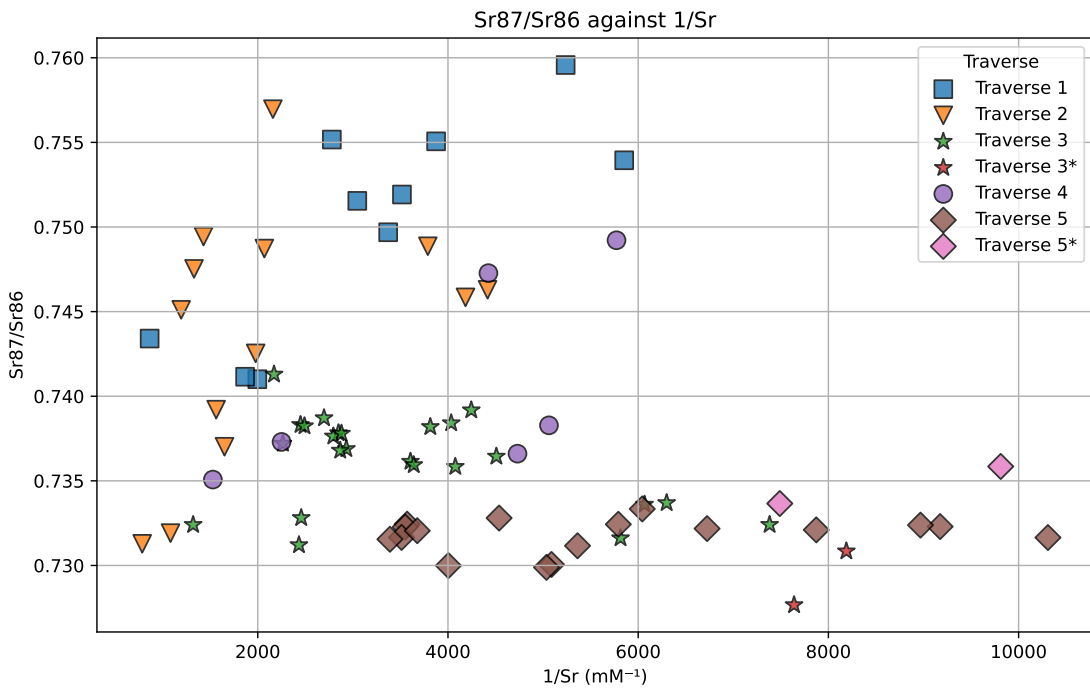


Figure 4: Strontium isotope differences display difference in lithology tapped in. Cite Quade and Tipper papers; Rain analysed for Sr isotopes and Cl. Something about contamination lower down; How samples of Traverse 3 compare to the rain samples

Sample ID	Elevation (m)	pH	$^{87}\text{Sr}/^{86}\text{Sr}$ (2SD·10 ⁶)	Sr (μM)	Cl (μM)	$\delta^{18}\text{O}$ (‰)	
NEP24-039	840	6.79	0.73906	(24)	0.13	28.09	-12.23
NEP24-043	1351	5.82	0.71442	(46)	0.01	3.55	-9.96
NEP24-044	1952	6.05	0.71352	(127)	0.01	1.89	-10.24
NEP24-045	2644	5.00	0.71292	(73)	0.01	3.21	-11.77
NEP24-046	2110	6.02	0.70904	(100)	0.02	2.86	-10.64
NEP24-047	2644	5.74	0.71194	(237)	0.01	0.55	-15.27
NEP24-048	2644	5.61	0.71182	(189)	0.01	3.65	-15.50

Table 2: Strontium isotope ratios, chloride and strontium concentrations (in micromolar, M), elevation, pH, and $\delta^{18}\text{O}$ values (‰ VSMOW). Error (2SD) values are multiplied by 10⁶.

Figure 4a shows $\frac{^{87}\text{Sr}}{^{86}\text{Sr}}$ against $\frac{1}{\text{Sr}}$ for springs in the catchment. The plot shows two distinct mixing lines between Traverses 1-3, and Traverses 3-5 [need to draw them on]. This supports that found in figure 3, which suggests the water chemistry in Traverses 1 and 2 is quite different to the trend set by Traverses 3-5. Comparing spring samples to the rain [Change graph], it is clear that the latter does not exert a significant control on the spring chemistry, not even for the presumably shortest flow paths at the top of the ridge. In other words, chemical weathering reactions are likely to be the main control on the spring chemistry.

5.4 Consistent Flow Paths Mid-Catchment

It is difficult to explain the inter-traverse variation in concentration and isotopic composition. As a result, for the remainder of this study's analysis, only Traverse 3 out of the five will be chosen as a case study representing the catchment. It is possible, and quite likely given the aforementioned mixing trends that all traverses' flow paths are connected one to the other. However, focusing on one traverse allows the contribution of spatial variation toward the overall chemistry to be minimised.

For Traverse 3, there is evidence to suggest lithology is largely constant. For one, geological maps suggest lithology does not vary across E-W, which is the profile all traverses follow. Secondly, the narrow range and tight scatter in Figure 5 for Na/Si suggests little lithological change and consistently sampled flow paths over time. Na/Si plots almost exactly on the 1:1 line for every season where the same spring was sampled in Traverse 3. The fact that this ratio increases with decreasing elevation makes sense given Si is involved in the backward secondary mineral precipitation weathering reaction, and Na is not. In other words, elevated Na/Si is interpreted as a sign of a closer approach to equilibrium, as more Si is scavenged from the water to form secondary precipitates, while the Na is only involved in dissolution. This is even more apparent when plotting against elevation.

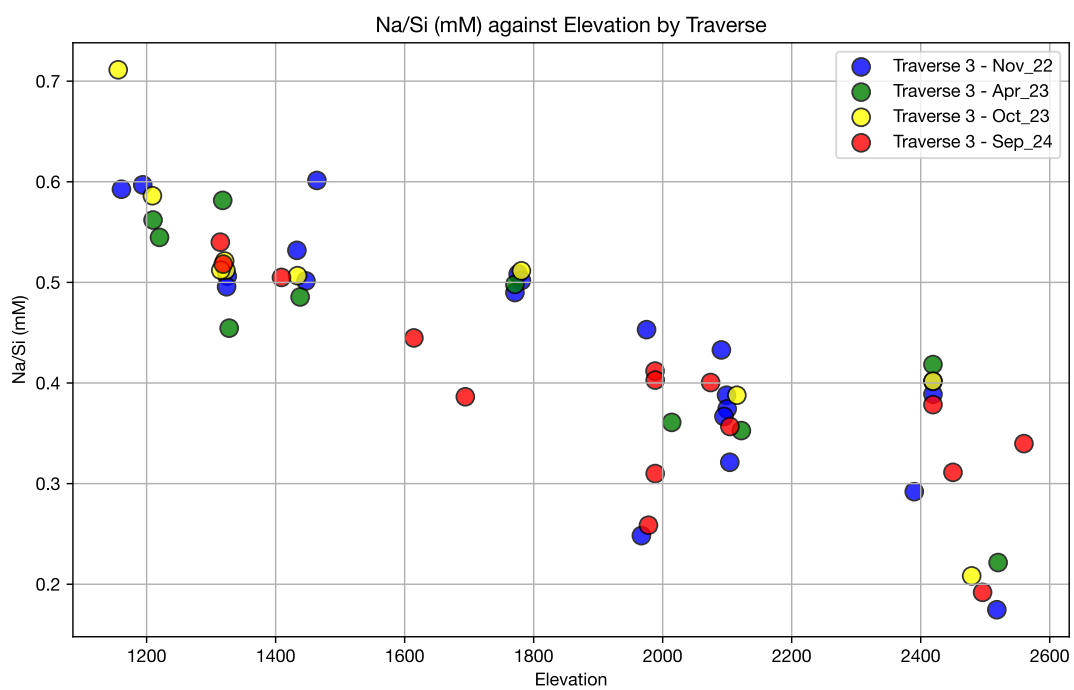
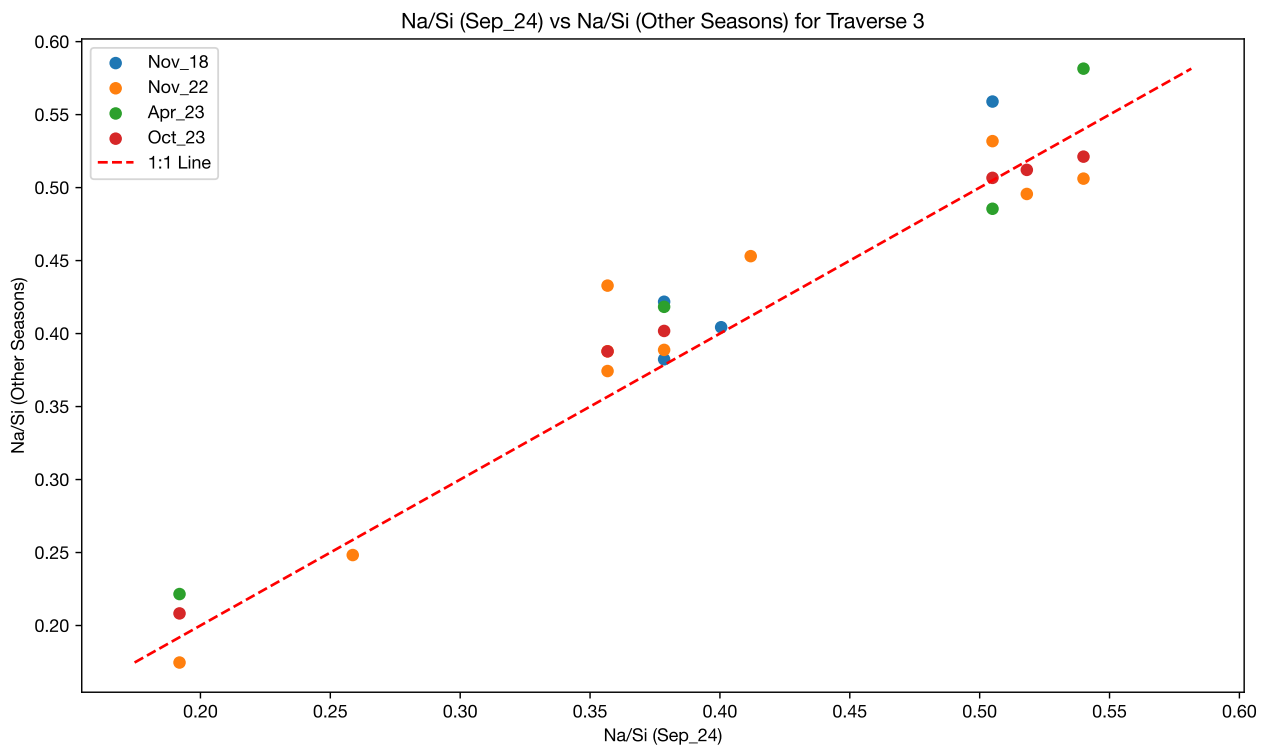


Figure 5: How Si varies for Traverse 3, showing a wide variety of samples; Na/Si for Traverse 3 is pretty neat. Consistently sampled flow paths.

Figure 6 shows the Na/Si ratio for the springs sampled over a time series. The Thalo spring exists in Traverse 3. The three springs displayed in Figure 6 largely follow the same spatial Na/Si trend as that shown in 5 (plot needed to show the spatial extent in Figure 5). An outlier, however, is the spike in Na/Si shortly after the start of the monsoon, suggesting temporal variation in flow paths. There is an argument to be made for this to be a spurious measurement due to its very large deviation from the other samples in the Thalo time-series. The spike is not just formed by one point, though. Around it the sampled points form a trough of sorts, suggesting that there is an approach to a high Na/Si signature. This spike is interpreted as the mobilisation of more concentrated, older water in the subsurface due to an increased water flux. In other words, the increased precipitation from the monsoon leads to flowpaths that sample deeper, older water that is closer to equilibrium.

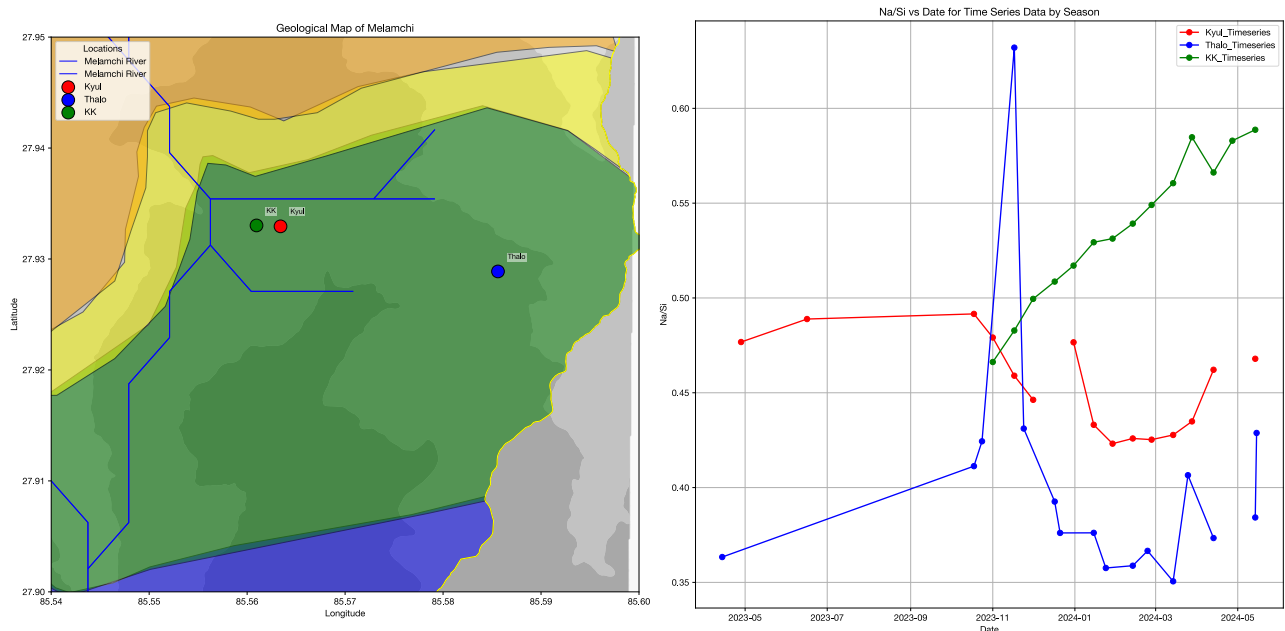


Figure 6: Na/Si for Thalo Timeseries

Traverse 3 therefore has consistent flow paths, scope for reactive transport modeling, and displays temporal variation in response to monsoonal precipitation. This makes it the optimal traverse for modeling the catchment.

6 Discussion

6.1 Modal Decomposition Identifies Weathering Reaction

The first step towards quantifying the extent to which chemical weathering reactions have gone to completion is to discern what reaction is taking place. In principle this is as simple as knowing what minerals are dissolving and which are precipitating. Modal decomposition methods consider several minerals that could be dissolving and/or precipitating, and their stoichiometry (Garrels and Mackenzie, 1967; Drever, 1997).

$$\begin{array}{ccccccccc}
 & Biot & Plag & Calc & Smec & Kaol & Kspar & Spring(\mu\text{mol/l}) \\
 Si & a_{11} & a_{12} & a_{13} & a_{14} & a_{15} & a_{16} & b_1 \\
 Al & a_{21} & a_{22} & a_{23} & a_{24} & a_{25} & a_{26} & b_2 \\
 Mg & a_{31} & a_{32} & a_{33} & a_{34} & a_{35} & a_{36} & b_3 \\
 Ca & a_{41} & a_{42} & a_{43} & a_{44} & a_{45} & a_{46} & b_4 \\
 Na & a_{51} & a_{52} & a_{53} & a_{54} & a_{55} & a_{56} & b_5 \\
 K & a_{61} & a_{62} & a_{63} & a_{64} & a_{65} & a_{66} & b_6
 \end{array} = \begin{pmatrix} x_{Biot} \\ x_{Plag} \\ x_{Calc} \\ x_{Smec} \\ x_{Kaol} \\ x_{Kspar} \end{pmatrix}$$

Matrix algebra facilitates the calculations of the mineral proportions in the water. Given known matrices A and B :

$$AX = B \quad (10)$$

$$X = A^{-1}B \quad (11)$$

This way, volumetric proportions of the minerals in the water can be calculated. Modal decomposition for spring waters was performed according to stoichiometric proportions from Bickle et al. (2015). For ease of visualisation, Figure 6 shows the positive, dissolved minerals on the LHS, and the negative, precipitated minerals on the RHS. [Bar Chart here](#)

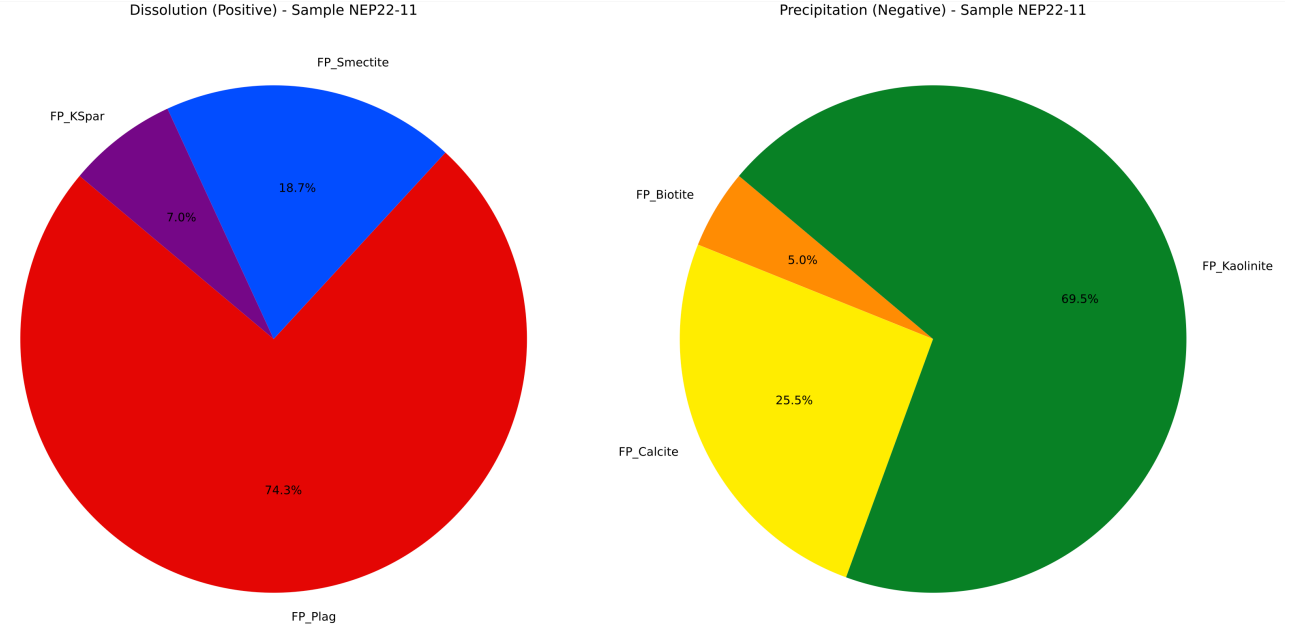
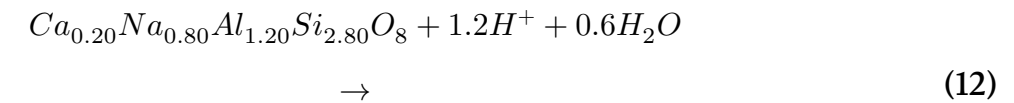
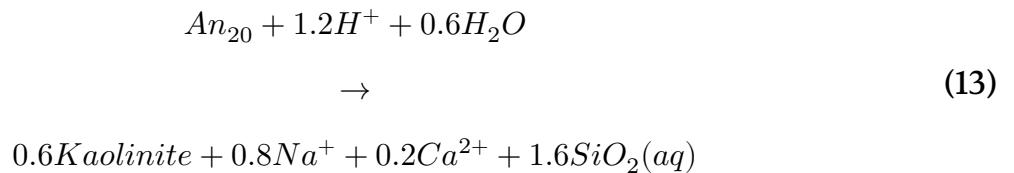


Figure 7: Example dissolution plot

Figure 6 is representative of most springs in Traverse 3. Hence, the major phase being dissolved is plagioclase feldspar and the major phase being precipitated is kaolinite. The primary composition of plagioclase in the area corresponds to \approx An-20 (Bickle et al., 2015; Knight et al., 2024). The plagioclase to kaolinite reaction is given by the following equation (written so that aluminium is conserved):



Or



6.2 One-Dimensional Reactive Transport Models

Reactive transport models are widely used in applied fluid dynamics and various fields within Earth Sciences. These models aim to track chemical reactions occurring at each spatial point, accounting for the movement of reactants to and reaction products away from those points (Bethke, 2011). The basic form of a reactive transport model is a partial differential equation that describes the transport of solutes and the reactions that occur between them. For reacting solutes, concentration changes over time are governed by transport rates—derived from the divergence principle—and the rate at which the component is introduced to or removed from the groundwater **Dissolution and Precipitation** (Bethke, 2011). The proposed equations can be complex, but in simple cases a species can be modelled to follow a first-order rate law, generally represented by **for an element concentration C_i :**

$$\frac{\partial C_i}{\partial t} = \mathcal{O}_T(C_i) + \mathcal{O}_R(C_i) \quad (14)$$

Where \mathcal{O}_T and \mathcal{O}_R are the transport and reaction operators, respectively (Bethke, 2011). Depending on the hypothesis supported, equation 14 can be modified accordingly. The following sections will discuss two models with their own versions of equation 14.

6.2.1 Model Motivation - **Do we add this into the other thing?**

As discussed in the introduction, there are different hypotheses regarding the major controls on chemical weathering. This section will contrast one model following the traditional, or "null" hypothesis that weathering is largely sensitive to climate and temperature (Fontorbe et al., 2013), and another model that suggests weathering is more sensitive to fluid flux (Maher, 2011; Maher and Chamberlain, 2013). Given the emphasis on deriving fluid residence times from solute concentrations, the benchmark for a model's effectiveness will be how well it can predict these times compared to previous studies on gas tracers and simple box models. Assumptions and constraints will be compared and contrasted, and their results used to inform the calculation of rates of reaction and approach to equilibrium in Melamchi. **Why do we use Si?**

6.2.2 Fontorbe et al. (2013) - Null Hypothesis - Model

This model investigates silicon isotopic composition in the Ganges River, assuming constant reaction rates along flow paths (see Appendix for a full derivation). **And see table on next part for derivation**

The first-order differential equation governing transport and reaction is given as:

$$\phi \frac{\partial C}{\partial t} = -\omega \phi \frac{\partial C}{\partial z} + R_n(1-f) \quad (15)$$

The equation can be nondimensionalised using the Damköhler number (N_D), which describes the relative importance of kinetic vs transport-controlled settings (Bethke, 2008)

Say what everything:

$$N_D = \frac{R_n h}{\phi C_o \omega} \quad (16)$$

Assuming steady-state ($\partial C / \partial t = 0$), the concentration at the end of the flow path can be rearranged to give the residence time T_f and reaction rate R_n :

$$T_f = \frac{(C - C_o)\phi}{(1 - f)R_n}; \quad R_n = \frac{(C - C_o)\phi}{(1 - f)T_f} \quad (17)$$

Fontorbe			
Parameter	Definition	Units	Formula (Value)
ϕ	Porosity	-	-
ω	Fluid velocity	m/s	-
h	Length of flow path	m	Variable
C	Concentration end of flow path	$\mu\text{mol/L}$	Variable
C_0	Initial concentration	$\mu\text{mol/L}$	Rain Conc
f	Fraction reprecipitated	-	Order 0.5 constant?
N_D	Non-dimensional number	-	$N_D = \frac{R_n h}{\phi C_0 \omega}$
T_f	Residence time	10^{-9} s	$T_f = \frac{h}{\omega}$
R_n	Reaction rate	$\text{mol/m}^3/\text{s}$	$k \cdot S \cdot \rho \cdot 1000 \cdot X$
k	Reaction rate constant	$\text{mol/m}^2/\text{s}$	-
S	Specific surface area	m^2/g	-
ρ	Mineral density	kg/m^3	
X	Volume fraction of mineral in rock	g_{min}/g_{rock}	0.2

Table 3: Key parameters and definitions for the Fontorbe model.

6.2.3 Maher Model - **Correct this with respect to mike**

This model is built to simulate hydrological processes controlling silicate weathering. The model is based on the assumption that the reaction rate decreases linearly with approach to equilibrium. The motivation behind the hydrological control is based on sensitivity analyses of real catchment data on one-dimensional reactive transport models that this study will be investigating, which suggest that porosity, mineral surface area, and temperature have no consistent correlation with water composition (Maher, 2011). The model begins with the following representation of the concentration of a solute in a fluid flow path:

$$\frac{dc}{dt} = -\frac{q}{\theta} \frac{dc}{dx} + \sum_i \mu_i R_{d,i} \left(1 - \left(\frac{c}{c_{eq}} \right)^{n_i} \right)^{m_i} - \sum_i \mu_i R_{p,i} \left(1 - \left(\frac{c}{c_{eq}} \right)^{n_i} \right)^{m_i} \quad (18)$$

Where c is the concentration **of the element**, q is the fluid flux, θ is the volumetric water content, x is the position along the flow path, μ is the stoichiometric coefficient, R is the rate of reaction for dissolution and precipitation respectively, c_{eq} is the concentration at equilibrium, and n and m are non-linear parameters (Maher and Chamberlain, 2013). Maher and Chamberlain describe that the reaction rate decreases linearly with approach to equilibrium. **Rn is defined as:**

$$R_n = \sum_i \mu_i R_{d,i} - \sum_i \mu_i R_{p,i} \quad (19)$$

$$\frac{dc}{dt} = R_n \left(1 - \frac{c}{c_{eq}} \right) \quad (20)$$

This can be solved for c , and rearranged for residence time and the rate of reaction to obtain (following Maher and Chamberlain, 2013):

And note the e2 term because it simulates to equilibrium eg

$$T_f = \frac{C_{eq} \cdot (C - C_0)}{e^2 R_n (C_{\text{eq}} - C)}; \quad R_n = \frac{C_{eq} \cdot (C - C_0)}{e^2 T_f (C_{\text{eq}} - C)} \quad (21)$$

Maher			
Parameter	Definition	Units	Formula (Value)
L	Length of flow path	m	Variable
q	Flow rate	m/s	Variable
ϕ	Porosity	-	0.3 (but variable)
θ	Volumetric water content	-	Variable
R_n	Net reaction rate	mol/L/s	$\rho_{sf} \cdot k \cdot A \cdot X_r$
ρ_{sf}	Mass mineral / Fluid Volume ratio	g/L	$1000 \cdot \rho_b / \phi$
ρ_b	Plagioclase density	g/cm ³	-
k	Reaction rate constant	mol/m ² /s	-
A	Specific surface area	m ² /g	0.1-1
X_r	Mineral concentration in fresh rock	g _{min} /g _{rock}	Wt% in rock
τ	Scaling factor	-	$\tau = e^2$
D_w	Damkohler Coefficient	m ² /s	$D_w = \frac{L\phi R_n}{C_{eq}}$
T_f	Residence time	10 ⁻⁶ s	$T_f = \frac{L\phi}{q}$
C_{eq}	Equilibrium concentration	μmol/L	Max Catchment
C_0	Initial concentration	μmol/L	Rain Conc

Table 4: Key parameters and definitions for the Maher model.

6.2.4 Comparison of the Models

Fontorbe	Maher
$T_f = \frac{(C_h - C_o) \cdot \phi}{(1 - f) \cdot R_n}$	$T_f = \frac{C_{eq} \cdot (C - C_0)}{e^2 R_n (C_{eq} - C)}$
$R_n = \frac{(C_h - C_o) \cdot \phi}{(1 - f) \cdot T_f}$	$R_n = \frac{C_{eq} \cdot (C - C_0)}{e^2 T_f (C_{eq} - C)}$

Table 5: Comparison of equations from Fontorbe and Maher

From this table comparison, it is easy to see the differences between why the two models will differ in their estimation of residence time. The difference in the models comes from the equilibrium concentration in the Maher formula. Indeed, given that the concentration is taken from the highest in the catchment (so as not to follow Maher and Chamberlain (2013)'s rather conservative estimate following Gaillardet et al. (1999)'s global river data)**rewrite in a nicer fashion**, the fraction

$$\frac{C_{eq}}{C_{eq} - C}$$

gets larger as the reaction progresses. As the reaction progresses, the Maher model will predict longer times than the Fontorbe model.**More about the model differences**

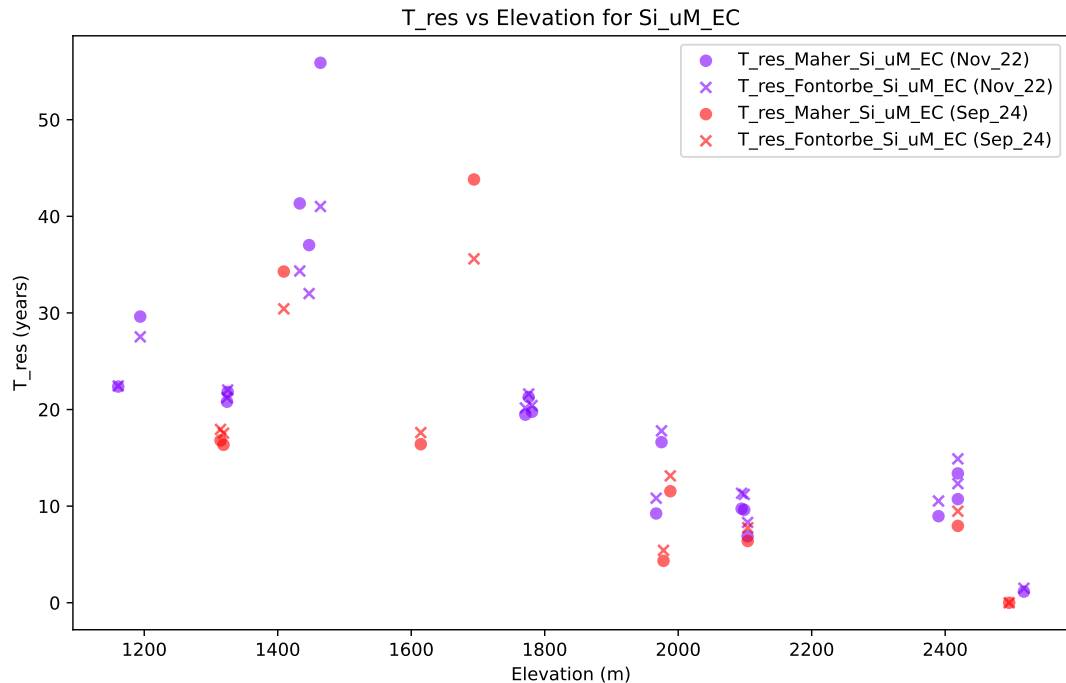


Figure 8: Comparison for the residence time between the two models. Evaluated for Specific surface area = 0.1; Mineral concentration in rock = 0.2; density of plagioclase = 2700; Reaction rate constant = 10e-15; Porosity = 0.1; Equilibrium concentration = Max in the catchment = 800 uM; Initial concentration = smallest in the traverse; Fraction reprecipitated = 0.5.

As expected, the Fontorbe model predicts older times at short flow paths, and the Maher model predicts older times at longer flow paths. This difference is due to the formulation of the rate of reaction, which is constant in the Fontorbe model but depends on the equilibrium concentration for the Maher model. Indeed, as equilibrium concentration is reached, the reaction rate will decrease, and the residence time will increase. It is unrealistic that reaction rate continue to be constant as the reaction progresses, and so the Maher model is more appropriate to describe catchment-wide settings such as this. This is illustrated in the following graphic: **But DO they approach equilibrium?? See next section eg**

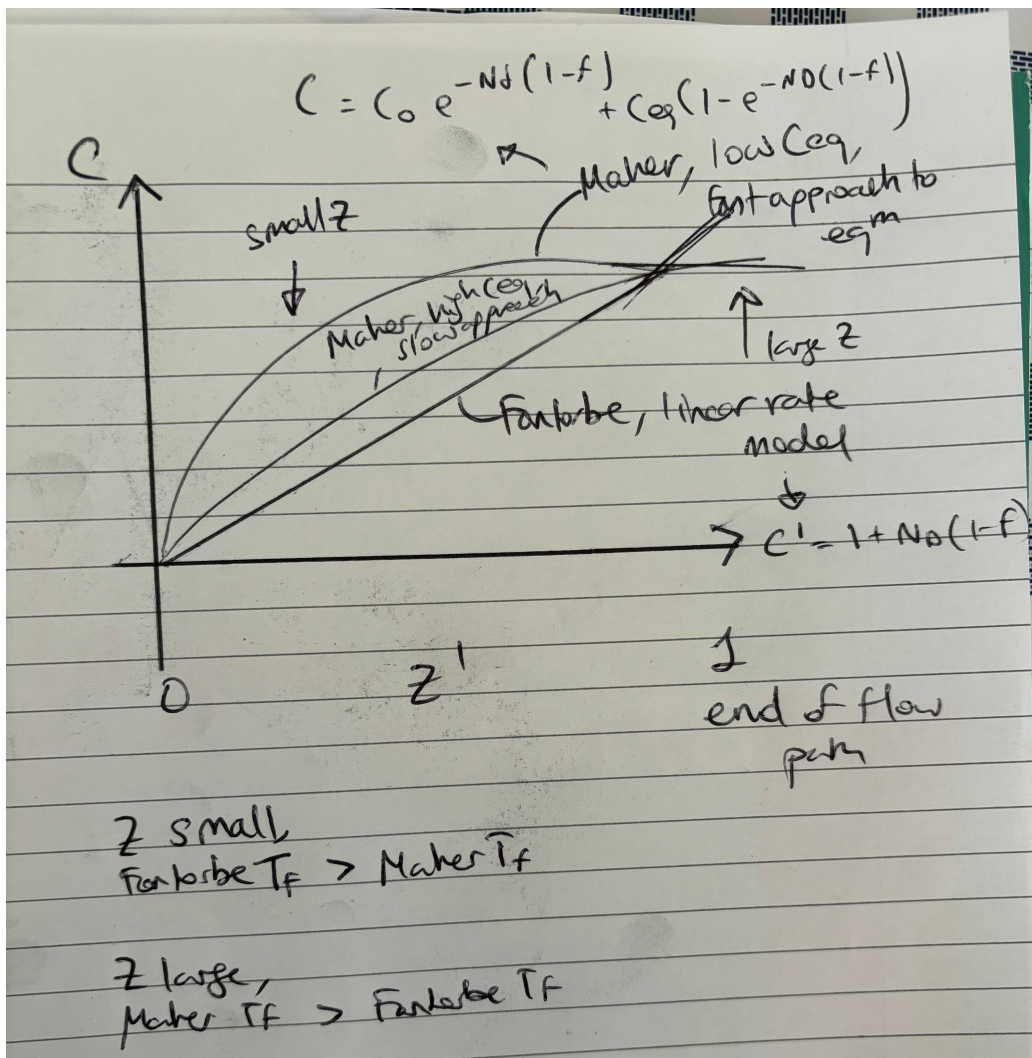


Figure 9: Comparison of how concentration changes with flow path length for the two models, and different equilibrium concentration

6.2.5 Constraints on Residence Time

As per Acharya et al. (2020), parts of the literature suggest that the most amount of precipitation occur in the top quarter of the Himalayan catchments. **see lit review eg** Studies analysing gas ages suggest that the residence time of the water in this catchment is on the order of 10 years, with an average of 25 years (Atwood et al, 2020).

Assuming an average rainfall rate of 3.5 m/yr (cite) over the top quarter of the catchment which is approximately 1km long, a m²/yr rate of 3500 is obtained. When considering a 10m wide channel flow of water, a flow rate of 350 m/yr for the top quarter of the catchment is obtained. **Need more meat on this..**

Secondly, using the oxygen isotopic composition of the springs, and comparing to the rainfall line, it is possible to obtain a flow path length assuming a general slope of 20 degrees:

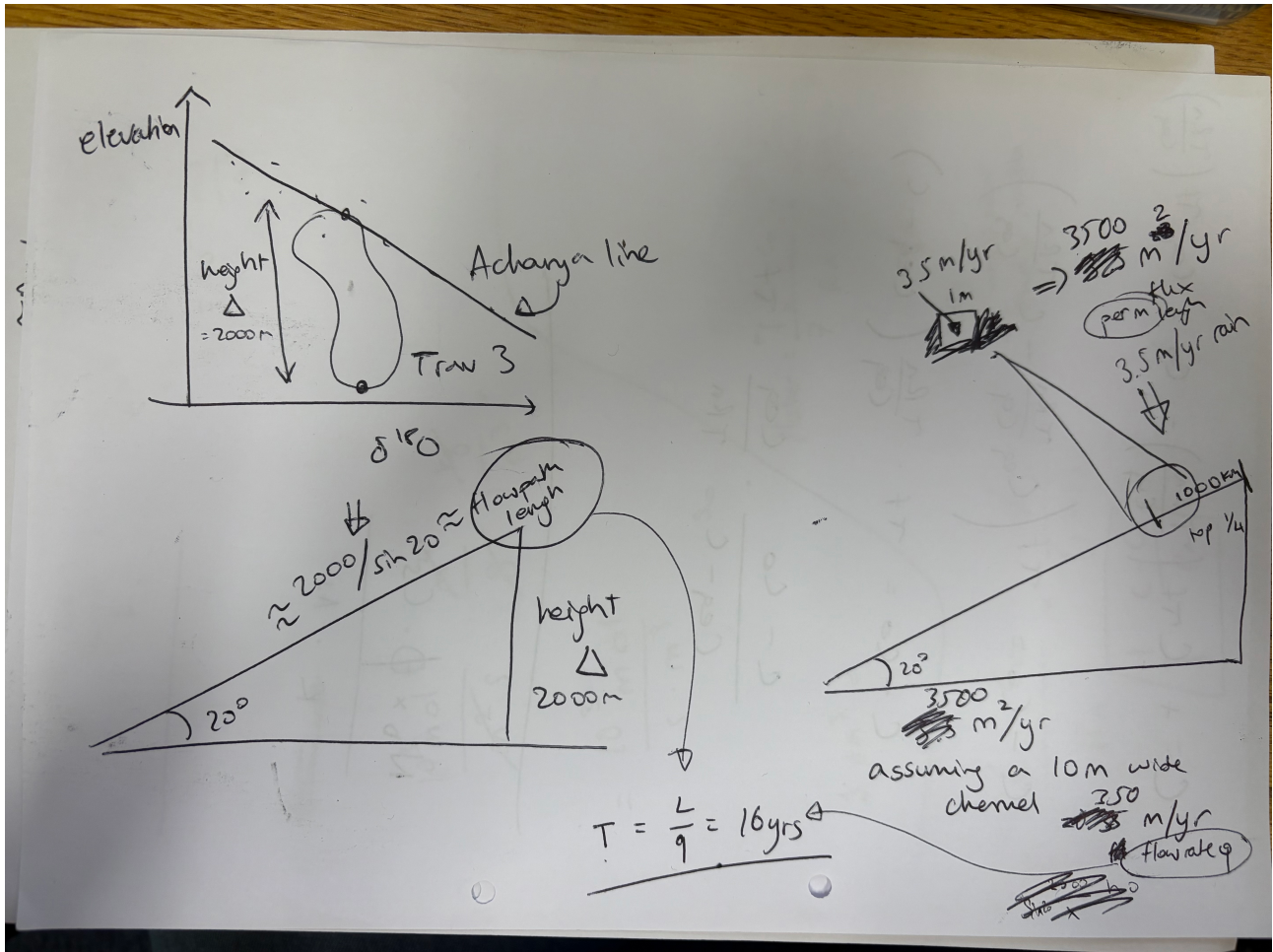


Figure 10: Proving the point that residence time is around 10 years

In this way it is plausible that 10 years could be how long the water is spending in the catchment, consistent with the **both** models. Such a finding suggests that the delay in river discharge of Andermann et al. (2013) is likely only recording surface or near-surface flow. The shorter flow paths here could plausibly be associated to residence times of a few months.

6.3 Free Energy Calculations

A further constraint on the approach to equilibrium of a water packet is the free energy of reaction, which can be calculated using the activity of the ions in solution. Free energy is defined as:[cite](#)

$$\Delta G = \Delta G^0 + RT \ln Q \quad (22)$$

The plagioclase to kaolinite reaction is given by equation 13. The parameters for the standard free energy of reaction are calculated using the pygcc python package ([cite](#)). The package gives the standard properties of solid-solution species and reactions, such that ΔG^0 can be calculated:

$$\Delta G^0 = \Delta G_{products}^0 - \Delta G_{reactants}^0 = -RT \ln K \quad (23)$$

K is calculated using the database obtained from pygcc using The Geochemist's Workbench® Rxn program. Q is calculated as the ion activity product of the reaction, assuming an ideal system whereby the activity is equal to the concentration of the ion in the water [Assuming the activities of the solid phases plagioclase and kaolinite are 1, the activity of water is 1, and the activity of the ions in solution are equal to their concentration, the free energy of reaction can be calculated.](#)

$$Q = \frac{a_{\text{Kaol}}^{0.6} a_{\text{Na}^+}^{0.8} a_{\text{Ca}^{2+}}^{0.2} a_{\text{SiO}_2(\text{aq})}^{1.6}}{a_{\text{An}_{20}} a_{\text{H}^+}^{1.2}} \quad (24)$$

It is important to note that the composition of the plagioclase is important. The free energy of reaction is lowered by the presence of a solid solution between albite and anorthite (Dubacq, 2022). [In our case...](#)

6.3.1 Comparison with Residence Time

Need to write

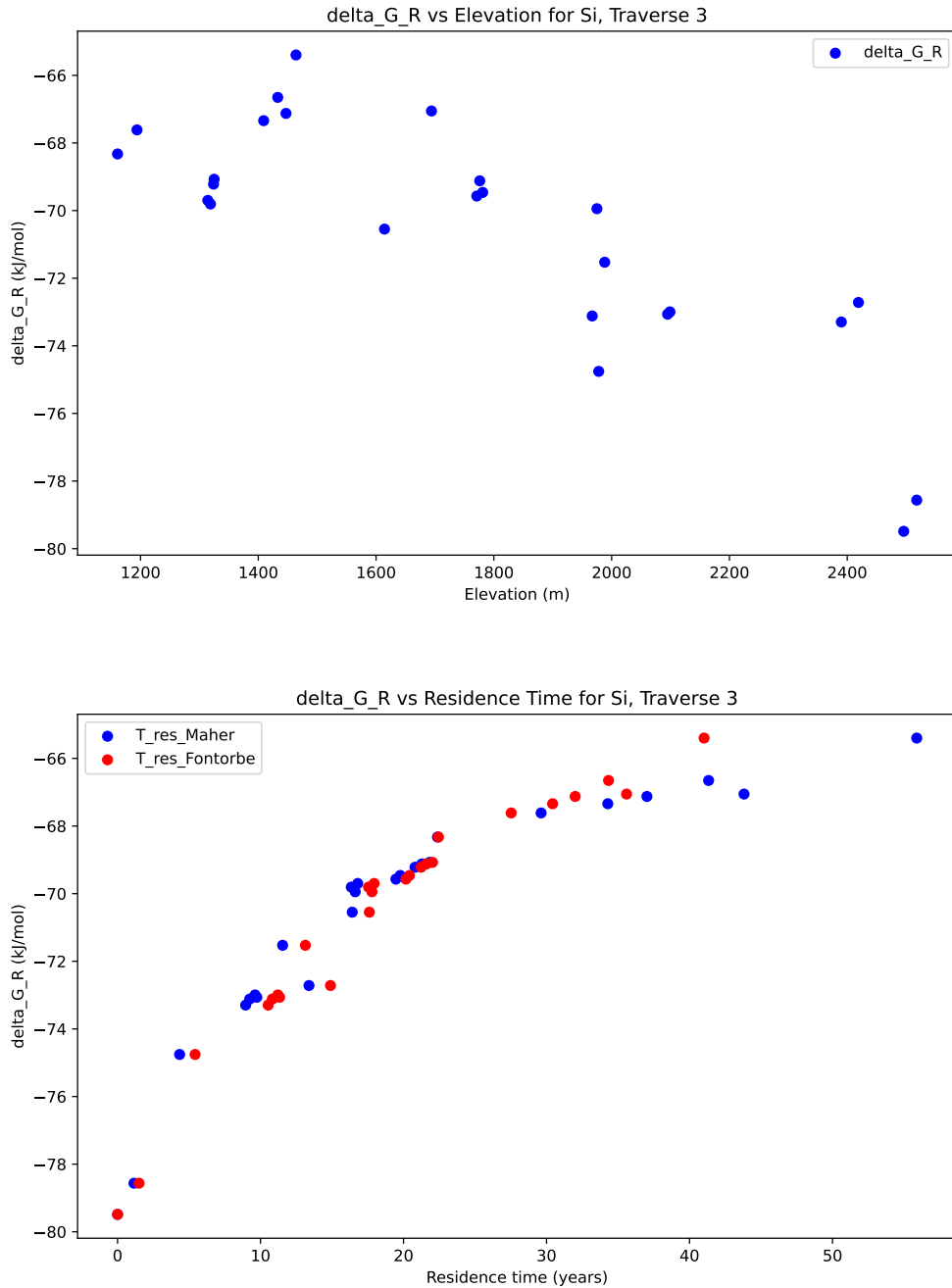


Figure 11: Comparison of the delta G obtained against elevation. Comparison of delta G with residence time for both models

6.3.2 Constraints on Reaction Rate

Figure 11 shows a convincing trend of decrease in ΔG as elevation decreases, consistent with the water samples getting closer to equilibrium as they flow for more time, and so the reaction occurs more. However, the free energy is only on the order of -60 kJ/mol at the longest flow path. This is not close to the -10kJ/mol that Kampman et al. (2014) suggest is the "near equilibrium plateau". There might be an argument, therefore, to suggest that the reaction rate is not as high as the models suggest. Indeed, at those values, laboratory rates might be more appropriate **Have the Kampman table? Lab rates of reaction are much faster for this**. One sure test is to compare the free energy obtained for the samples in Traverse 3 to those in Traverse 1. Given that the equilibrium concentration for the residence time is taken from this latter traverse (see Figure in results, ref), according to the formulation of the Maher model this should be closest to equilibrium.

Figure 12 does indeed show that the free energy of reaction is lower for the samples in Traverse 1 than in Traverse 3. However, the maximum value reached is still far away from equilibrium. Hence, it is likely that a larger reaction rate is needed to characterise these groundwaters. This has implications for the residence times calculated using these models, as the former and latter are inversely proportional.

**Bit about Maher assuming equilibrium reached -> Maher not correct to implement here.
Also mike permeability sketch???**

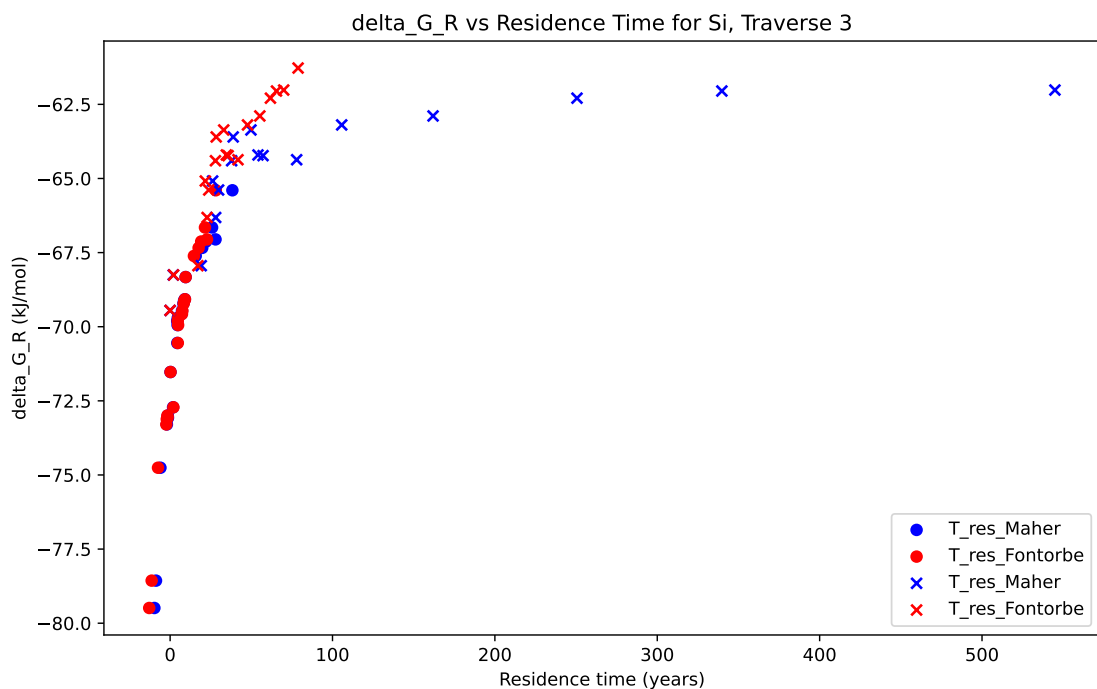
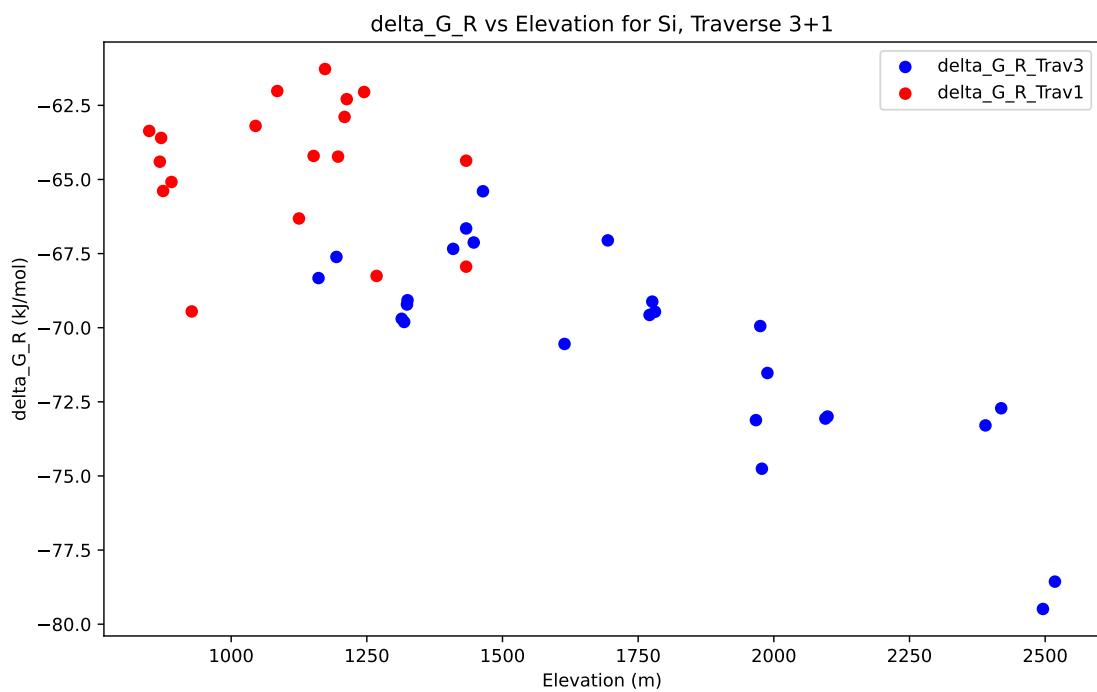


Figure 12: Comparison of the delta G obtained against elevation for Traverse 1 and Traverse 3. And residence time comparison, Note how Maher predicts really high residence times when Ceq is approached

References

- [1] Open-file report. Series: Open-File Report.
- [2] Sunil Acharya, Xiaoxin Yang, Tandong Yao, and Dibas Shrestha. Stable isotopes of precipitation in nepal himalaya highlight the topographic influence on moisture transport. 565:22–30.
- [3] Tirtha Raj Adhikari, Binod Baniya, QiuHong Tang, Rocky Talchabhadel, Manish Raj Gouli, Bhumi Raj Budhathoki, and Ram Prasad Awasthi. Evaluation of post extreme floods in high mountain region: A case study of the melamchi flood 2021 at the koshi river basin in nepal. 3(3):437–446.
- [4] Christoff Andermann, Laurent Longuevergne, Stéphane Bonnet, Alain Crave, Philippe Davy, and Richard Gloaguen. Impact of transient groundwater storage on the discharge of himalayan rivers. 5(2):127–132.
- [5] C. A. J. Appelo and Dieke Postma. Geochemistry, groundwater and pollution. CRC Press, 2nd ed., 5th corr. repr edition.
- [6] Abra Catherine Atwood. Critical zone response to perturbation: from mountain building to wildfire.
- [7] Binod Baniya, QiuHong Tang, Tirtha Raj Adhikari, Gang Zhao, Gebremedhin Gebremeskel Haile, Madan Sigdel, and Li He. Climate change induced melamchi extreme flood and environment implication in central himalaya of nepal. 120(12):11009–11029.
- [8] Paolo Benettin, Scott W. Bailey, John L. Campbell, Mark B. Green, Andrea Rinaldo, Gene E. Likens, Kevin J. McGuire, and Gianluca Botter. Linking water age and solute dynamics in streamflow at the hubbard brook experimental forest, NH, USA. 51(11):9256–9272.

- [9] Craig M Bethke. GEOCHEMICAL AND BIOGEOCHEMICAL REACTION MODELING, second edition.
- [10] M.J. Bickle, E. Tipper, A. Galy, H. Chapman, and N. Harris. On discrimination between carbonate and silicate inputs to himalayan rivers. 315(2):120–166.
- [11] Bodo Bookhagen and Douglas W. Burbank. Toward a complete himalayan hydrological budget: Spatiotemporal distribution of snowmelt and rainfall and their impact on river discharge. 115:2009JF001426.
- [12] Jesús Carrera, Maarten W. Saaltink, Joaquim Soler-Sagarra, Jingjing Wang, and Cristina Valhondo. Reactive transport: A review of basic concepts with emphasis on biochemical processes. 15(3):925.
- [13] Mingkun Chen, Lei Gong, Jacques Schott, Peng Lu, Kaiyun Chen, Honglin Yuan, Jian Sun, Si Athena Chen, John Apps, and Chen Zhu. Coupled feldspar dissolution and secondary mineral precipitation in batch systems: 6. labradorite dissolution, calcite growth, and clay precipitation at 60 °c and pH 8.2–8.4. 390:181–198.
- [14] Christian David, Teng-Fong Wong, Wenlu Zhu, and Jiaxiang Zhang. Laboratory measurement of compaction-induced permeability change in porous rocks: Implications for the generation and maintenance of pore pressure excess in the crust. 143(1):425–456.
- [15] Megh Raj Dhital. Geology of the Nepal Himalaya. Regional Geology Reviews. Springer International Publishing.
- [16] Jennifer L. Druhan and Kate Maher. The influence of mixing on stable isotope ratios in porous media: A revised rayleigh model. 53(2):1101–1124.
- [17] Benoît Dubacq. Thermodynamics of ordering and mixing in plagioclase feldspars: atomistic modelling in favour of landau theory. 177(10):102.
- [18] Guillaume Fontorbe, Christina L. De La Rocha, Hazel J. Chapman, and Michael J. Bickle. The silicon isotopic composition of the ganges and its tributaries. 381:21–30.

- [19] J. Gaillardet, B. Dupré, P. Louvat, and C.J. Allègre. Global silicate weathering and CO₂ consumption rates deduced from the chemistry of large rivers. 159(1):3–30.
- [20] Albert Galy, Christian France-Lanord, and Louis A Derry. The strontium isotopic budget of himalayan rivers in nepal and bangladesh. 63(13):1905–1925.
- [21] R.B. Georg, B.C. Reynolds, A.J. West, K.W. Burton, and A.N. Halliday. Silicon isotope variations accompanying basalt weathering in iceland. 261(3):476–490.
- [22] R.B. Georg, B.C. Reynolds, A.J. West, K.W. Burton, and A.N. Halliday. Silicon isotope variations accompanying basalt weathering in iceland. 261(3):476–490.
- [23] Jon K. Golla, Marie L. Kuessner, Michael J. Henehan, Julien Bouchez, Daniella M. Rempe, and Jennifer L. Druhan. The evolution of lithium isotope signatures in fluids draining actively weathering hillslopes. 567:116988.
- [24] Bradley W. Goodfellow, George E. Hilley, Samuel M. Webb, Leonard S. Sklar, Seulgi Moon, and Christopher A. Olson. The chemical, mechanical, and hydrological evolution of weathering granitoid. 121(8):1410–1435.
- [25] Emma L. S. Graf, Hugh D. Sinclair, Mikael Attal, Boris Gailleton, Basanta Raj Adhikari, and Bishnu Raj Baral. Geomorphological and hydrological controls on sediment export in earthquake-affected catchments in the nepal himalaya.
- [26] Danielle K. Hare, Ashley M. Helton, Zachary C. Johnson, John W. Lane, and Martin A. Briggs. Continental-scale analysis of shallow and deep groundwater contributions to streams. 12(1):1450.
- [27] Madeline M Hille. The orographic influence on storm variability, extreme rainfall characteristics and rainfall-triggered landsliding in the central nepalese himalaya.
- [28] T.J. B. Holland and R. Powell. An improved and extended internally consistent thermodynamic dataset for phases of petrological interest, involving a new equation of state for solids: THERMODYNAMIC DATASET FOR PHASES OF PETROLOGICAL INTEREST. 29(3):333–383.

- [29] L. Illien, C. Andermann, C. Sens Schönfelder, K. L. Cook, K. P. Baidya, L. B. Adhikari, and N. Hovius. Subsurface moisture regulates himalayan groundwater storage and discharge. 2(2):e2021AV000398.
- [30] Scott Jasechko. Global isotope hydrogeology review. 57(3):835–965.
- [31] Scott Jasechko. Partitioning young and old groundwater with geochemical tracers. 427:35–42.
- [32] A. Joshua West, Mike J. Bickle, Rob Collins, and James Brasington. Small-catchment perspective on himalayan weathering fluxes. 30(4):355.
- [33] Pratik Kad and Kyung Ja Ha. Recent tangible natural variability of monsoonal orographic rainfall in the eastern himalayas. 128(22):e2023JD038759.
- [34] Niko Kampman, Mike Bickle, John Becker, Nelly Assayag, and Hazel Chapman. Feldspar dissolution kinetics and gibbs free energy dependence in a CO₂-enriched groundwater system, green river, utah. 284(3):473–488.
- [35] D. B. Kattel, T. Yao, K. Yang, L. Tian, G. Yang, and D. Joswiak. Temperature lapse rate in complex mountain terrain on the southern slope of the central himalayas. 113(3):671–682.
- [36] Julia L. A. Knapp, Colin Neal, Alessandro Schlumpf, Margaret Neal, and James W. Kirchner. New water fractions and transit time distributions at plynlimon, wales, estimated from stable water isotopes in precipitation and streamflow. 23(10):4367–4388.
- [37] Alasdair C.G. Knight, Emily I. Stevenson, Luke Bridgestock, J. Jotautas Baronas, William J. Knapp, Basanta Raj Adhikari, Christoff Andermann, and Edward T. Tipper. The impact of adsorption–desorption reactions on the chemistry of himalayan rivers and the quantification of silicate weathering rates. 641:118814.
- [38] Lee R. Kump, Susan L. Brantley, and Michael A. Arthur. Chemical weathering, atmospheric CO₂, and climate. 28(1):611–667.

- [39] Başak Kısakürek, Rachael H. James, and Nigel B.W. Harris. Li and δ^{7Li} in himalayan rivers: Proxies for silicate weathering? 237(3):387–401.
- [40] K. Maher. The dependence of chemical weathering rates on fluid residence time. 294(1):101–110.
- [41] K. Maher. The role of fluid residence time and topographic scales in determining chemical fluxes from landscapes. 312(1):48–58.
- [42] K. Maher and C. P. Chamberlain. Hydrologic regulation of chemical weathering and the geologic carbon cycle. 343(6178):1502–1504.
- [43] K. Maher and C. P. Chamberlain. Hydrologic regulation of chemical weathering and the geologic carbon cycle. 343(6178):1502–1504.
- [44] Kate Maher, Carl I. Steefel, Art F. White, and Dave A. Stonestrom. The role of reaction affinity and secondary minerals in regulating chemical weathering rates at the santa cruz soil chronosequence, california. 73(10):2804–2831.
- [45] Katharine Maher, Donald J. DePaolo, and Jo Chiu-Fang Lin. Rates of silicate dissolution in deep-sea sediment: In situ measurement using $^{234}U/^{238}U$ of pore fluids. 68(22):4629–4648.
- [46] Odin Marc, Robert Behling, Christoff Andermann, Jens M. Turowski, Luc Illien, Sigrid Roessner, and Niels Hovius. Long-term erosion of the nepal himalayas by bedrock landsliding: the role of monsoons, earthquakes and giant landslides. 7(1):107–128.
- [47] James L. McCallum, Peter G. Cook, and Craig T. Simmons. Limitations of the use of environmental tracers to infer groundwater age. 53:56–70.
- [48] K. J. McGuire, J. J. McDonnell, M. Weiler, C. Kendall, B. L. McGlynn, J. M. Welker, and J. Seibert. The role of topography on catchment scale water residence time. 41(5):2004WR003657.
- [49] William G. Medwedeff, Marin K. Clark, Dimitrios Zekkos, A. Joshua West, and Deepak Chamlagain. Near surface geomechanical properties and weathering char-

acteristics across a tectonic and climatic gradient in the central nepal himalaya. 127(2):e2021JF006240.

- [50] Jeeban Panthi, Piyush Dahal, Madan Shrestha, Suman Aryal, Nir Krakauer, Soni Pradhanang, Tarendra Lakhankar, Ajay Jha, Mohan Sharma, and Ramchandra Karki. Spatial and temporal variability of rainfall in the gandaki river basin of nepal himalaya. 3(1):210–226.
- [51] Michelle A. Pedrazas, W. Jesse Hahm, Mong Han Huang, David Dralle, Mariel D. Nelson, Rachel E. Breunig, Kristen E. Fauria, Alexander B. Bryk, William E. Dietrich, and Daniella M. Rempe. The relationship between topography, bedrock weathering, and water storage across a sequence of ridges and valleys. 126(4):e2020JF005848.
- [52] Jay Quade, Nathan English, and Peter G DeCelles. Silicate versus carbonate weathering in the himalaya: a comparison of the arun and seti river watersheds. 202(3):275–296.
- [53] Kevin Roback, Marin K. Clark, A.Joshua West, Dimitrios Zekkos, Gen Li, Sean F. Gallen, Deepak Chamlagain, and Jonathan W. Godt. The size, distribution, and mobility of landslides caused by the 2015 mw7.8 gorkha earthquake, nepal. 301:121–138.
- [54] Joaquim Soler-Sagarra, Maarten W. Saaltink, Francesca De Gaspari, Albert Nardi, and Jesús Carrera. Water mixing approach (WMA) for reactive transport modeling.
- [55] Matthias Sprenger, Christine Stumpp, Markus Weiler, Werner Aeschbach, Scott T. Allen, Paolo Benettin, Maren Dubbert, Andreas Hartmann, Markus Hrachowitz, James W. Kirchner, Jeffrey J. McDonnell, Natalie Orlowski, Daniele Penna, Stephan Pfahl, Michael Rinderer, Nicolas Rodriguez, Maximilian Schmidt, and Christiane Werner. The demographics of water: A review of water ages in the critical zone. 57(3):800–834.
- [56] R. F. Stallard and J. M. Edmond. Geochemistry of the amazon: 2. the influence of geology and weathering environment on the dissolved load. 88:9671–9688.

- [57] Philip A. E. Pogge Von Strandmann, Mathieu Dellinger, and A. Joshua West. Lithium Isotopes: A Tracer of Past and Present Silicate Weathering. Cambridge University Press, 1 edition.
- [58] Nicholas E. Thiros, Erica R. Siirila Woodburn, P. James Dennedy Frank, Kenneth H. Williams, and W. Payton Gardner. Constraining bedrock groundwater residence times in a mountain system with environmental tracer observations and bayesian uncertainty quantification. 59(2):e2022WR033282.
- [59] Edward T Tipper. The isotopic fingerprint of calcium and magnesium: from the alteration of the continental crust to global budgets.
- [60] Edward T. Tipper, Mike J. Bickle, Albert Galy, A. Joshua West, Catherine Pomiès, and Hazel J. Chapman. The short term climatic sensitivity of carbonate and silicate weathering fluxes: Insight from seasonal variations in river chemistry. 70(11):2737–2754.
- [61] Rong Wen, LiDe Tian, YongBiao Weng, ZhongFang Liu, and ZhongPing Zhao. The altitude effect of δ 18O in precipitation and river water in the southern himalayas. 57(14):1693–1698.
- [62] A West, A Galy, and M Bickle. Tectonic and climatic controls on silicate weathering. 235(1):211–228.
- [63] A. J. West, M. Arnold, G. Aumaître, D. L. Bourlès, K. Keddadouche, M. Bickle, and T. Ojha. High natural erosion rates are the backdrop for present-day soil erosion in the agricultural middle hills of nepal. 3(3):363–387.
- [64] Art F. White, Alex E. Blum, Marjorie S. Schulz, Tom D. Bullen, Jennifer W. Harden, and Maria L. Peterson. Chemical weathering rates of a soil chronosequence on granitic alluvium: I. quantification of mineralogical and surface area changes and calculation of primary silicate reaction rates. 60(14):2533–2550.
- [65] Art F White and Susan L Brantley. The effect of time on the weathering of silicate minerals: why do weathering rates differ in the laboratory and field? 202(3):479–506.

- [66] John A Wojtowicz. The thermodynamic basis of the saturation index.
- [67] Bing Xu, Aihong Xie, and Jiangping Zhu. Can water vapor transport over the himalayas above 8000 m asl?—a case study on mt. everest. 14(11):1671.

7 Appendix 1: Strontium Isotopes and their Applications

Need to include a blurb about how they originate and what they mean.

Following Faure (2001- Origin of Igneous Rocks), the Sr concentrations of a two-component mixture can be expressed as:

$$[Sr]_M = [Sr]_A f_A + [Sr]_B (1 - f_A) \quad (25)$$

These are related to the isotopic composition with:

$$\left(\frac{^{87}Sr}{^{86}Sr} \right)_M = \left(\frac{^{87}Sr}{^{86}Sr} \right)_A f_A \frac{[Sr]_A}{[Sr]_M} + \left(\frac{^{87}Sr}{^{86}Sr} \right)_B (1 - f_A) \frac{[Sr]_B}{[Sr]_M} \quad (26)$$

These equations can be combined, yielding:

$$\left(\frac{^{87}Sr}{^{86}Sr} \right)_M = \frac{a}{[Sr]_M} + b; \quad \text{with:} \quad (27)$$

$$a = \frac{[Sr]_A [Sr]_B \left[\left(\frac{^{87}Sr}{^{86}Sr} \right)_B - \left(\frac{^{87}Sr}{^{86}Sr} \right)_A \right]}{[Sr]_A - [Sr]_B} \quad (28)$$

$$b = \frac{[Sr]_A \left(\frac{^{87}Sr}{^{86}Sr} \right)_A - [Sr]_B \left(\frac{^{87}Sr}{^{86}Sr} \right)_B}{[Sr]_A - [Sr]_B} \quad (29)$$

Plots of $\frac{^{87}Sr}{^{86}Sr}$ against $\frac{1}{Sr}$ that yield straight lines are therefore indicative of mixing trends.

8 Appendix 2: Derivation of reactive transport Models

8.1 Fontorbe et al. (2013) - Null Hypothesis - Model Derivation

This model investigates silicon isotopic composition in the Ganges River, assuming constant reaction rates along flow paths.

The first-order differential equation governing transport and reaction is given as:

To simplify, we introduce non-dimensional variables:

$$\phi \frac{\partial C}{\partial t} = -\omega \phi \frac{\partial C}{\partial z} + R_n(1-f) \quad (30)$$

$$C' = \frac{C}{C_o}, \quad z' = \frac{z}{h}, \quad t' = \frac{t\omega}{h} \quad (31)$$

Rewriting Equation (1) using these new variables:

$$\frac{\partial C'}{\partial t'} = -\frac{\partial C'}{\partial z'} + N_D(1-f) \quad (32)$$

The Damköhler number (N_D) describes the relative importance of kinetic vs transport-controlled settings (Bethke, 2008):

$$N_D = \frac{R_n h}{\phi C_o \omega} \quad (33)$$

Assuming a quasi-stationary state ($\partial C'/\partial t' = 0$), we get:

$$C' = 1 + z' N_D(1-f) \quad (34)$$

At the end of the flow path ($z = h, z' = 1$), this simplifies to:

$$N_D = \frac{C' - 1}{1 - f} \quad (35)$$

The residence time of water along the flow path is:

$$T_f = \frac{h}{\omega} \quad (36)$$

At the end of the flow path:

$$\frac{R_n h}{\phi C_o \omega} = \frac{C'_h - 1}{1 - f} \quad (37)$$

$$\frac{R_n T_f}{\phi C_o} = \frac{C'_h - 1}{1 - f} \quad (38)$$

Solving for residence time T_f and reaction rate R_n :

$$T_f = \frac{(C_h - C_o)\phi}{(1 - f)R_n} \quad (39)$$

$$R_n = \frac{(C_h - C_o)\phi}{(1 - f)T_f} \quad (40)$$

C_h is the concentration at the end of the flow path, which is taken to be equal to the concentration of each spring C , assuming each spring represents a unique flow path. Convert T_f from 10^{-9} seconds to years for practical use.

Fontorbe			
Parameter	Definition	Units	Formula (Value)
ϕ	Porosity	-	-
ω	Fluid velocity	m/s	-
h	Length of flow path	m	Variable
C_h	Concentration end of flow path	$\mu\text{mol/L}$	Variable
C_0	Initial concentration	$\mu\text{mol/L}$	Rain Conc
f	Fraction reprecipitated	-	Order 0.5
N_D	Non-dimensional number	-	$N_D = \frac{R_n h}{\phi C_0 \omega}$
T_f	Residence time	10^{-9} s	$T_f = \frac{h}{\omega}$
R_n	Reaction rate	$\text{mol/m}^3/\text{s}$	$k \cdot S \cdot \rho \cdot 1000 \cdot X$
k	Reaction rate constant	$\text{mol/m}^2/\text{s}$	-
S	Specific surface area	m^2/g	-
ρ	Mineral density	kg/m^3	-
X	Volume fraction of mineral in rock	g_{min}/g_{rock}	0.2

Table 6: Key parameters and definitions for the Fontorbe model.

8.2 Maher Model Derivation

This model describes a reaction-based approach to solute transport, following Maher and Chamberlain (2013, 2014).

The first-order differential equation governing transport and reaction is:

$$\frac{dc}{dt} = -\frac{q}{\theta} \frac{dc}{dx} + \sum_i \mu_i R_{d,i} \left(1 - \left(\frac{c}{c_{eq}} \right)^{n_i} \right)^{m_i} - \sum_i \mu_i R_{p,i} \left(1 - \left(\frac{c}{c_{eq}} \right)^{n_i} \right)^{m_i} \quad (41)$$

Where c is the concentration, q is the fluid flux, θ is the volumetric water content, x is the position along the flow path, μ is the stoichiometric coefficient, R is the rate of reaction for dissolution and precipitation respectively, c_{eq} is the equilibrium concentration, and n and m are non-linear parameters (Maher and Chamberlain, 2013).

$$\frac{dc}{dx} = \frac{q}{\theta} \sum_i \mu_i R_{d,i} \left(1 - \left(\frac{c}{c_{eq}} \right)^{n_i} \right)^{m_i} - \frac{q}{\phi} \sum_i \mu_i R_{p,i} \left(1 - \left(\frac{c}{c_{eq}} \right)^{n_i} \right)^{m_i} \quad (42)$$

Defining the net reaction rate:

$$R_n = \sum_i \mu_i R_{d,i} - \sum_i \mu_i R_{p,i} \quad (43)$$

Maher and Chamberlain describe that the reaction

rate decreases linearly with approach to equilibrium.

$$\frac{dc}{dt} = R_n \left(1 - \frac{c}{c_{eq}} \right) \quad (44)$$

Solving for $c(x)$, following Maher and Chamberlain (2013):

$$c(x) = c_0 \exp \left(-\frac{R_n \theta x}{qc_{eq}} \right) + c_{eq} \left(1 - \exp \left(-\frac{R_n \theta x}{qc_{eq}} \right) \right) \quad (45)$$

We also define the residence time T_f :

$$T_f = \frac{L\phi}{q} \quad (46)$$

Thus, at residence time T_f :

$$c(T_f) = c_0 \exp\left(-\frac{R_n T_f}{c_{\text{eq}}}\right) + c_{\text{eq}} \left(1 - \exp\left(-\frac{R_n T_f}{c_{\text{eq}}}\right)\right) \quad (47)$$

Following Maher and Chamberlain (2014), this can be rewritten as:

$$C = \frac{C_0}{1 + \tau D_w/q} + C_{\text{eq}} \frac{\tau D_w/q}{1 + \tau D_w/q} \quad (48)$$

where:

$$\tau = e^2; \quad D_w = \frac{L\theta R_n}{C_{\text{eq}}} \quad (49)$$

Rewriting the equation:

$$C = \frac{C_0 + C_{\text{eq}} \cdot T_f (e^2 \cdot R_n / C_{\text{eq}})}{1 + T_f (e^2 \cdot R_n / C_{\text{eq}})} \quad (50)$$

Solving for residence time T_f , and reaction rate R_n

$$T_f = \frac{C_{\text{eq}} \cdot (C - C_0)}{e^2 R_n (C_{\text{eq}} - C)} \quad (51)$$

which can be compared to the Fontorbe model:

$$R_n = \frac{C_{\text{eq}} \cdot (C - C_0)}{e^2 T_f (C_{\text{eq}} - C)} \quad (52)$$

Note: Convert T_f from 10^{-3} s to years for practical use.

Maher Model Parameters			
Parameter	Definition	Units	Formula (Value)
L	Length of flow path	m	Variable
q	Flow rate	m/s	Variable
ϕ	Porosity	-	0.3 (but variable)
θ	Volumetric water content	-	Variable
R_n	Net reaction rate	mol/L/s	$\rho_{sf} \cdot k \cdot A \cdot X_r$
ρ_{sf}	Mass mineral / Fluid Volume ratio	g/L	$1000 \cdot \rho_b / \phi$
ρ_b	Plagioclase density	g/cm ³	-
k	Reaction rate constant	mol/m ² /s	-
A	Specific surface area	m ² /g	0.1-1
X_r	Mineral concentration in fresh rock	g_{min} / g_{rock}	Wt% in rock
τ	Scaling factor	-	$\tau = e^2$
D_w	Damkohler Coefficient	m ² /s	$D_w = \frac{L\phi R_n}{C_{eq}}$
T_f	Residence time	10^{-6} s	$T_f = \frac{L\phi}{q}$
C_{eq}	Equilibrium concentration	$\mu\text{mol}/\text{L}$	Max Catchment
C_0	Initial concentration	$\mu\text{mol}/\text{L}$	Rain Conc

Table 7: Key parameters and definitions for the Maher model.